Thermal energy storage for nuclear power applications

by

Jacob N. Edwards

B.S., Kansas State University, 2014

A THESIS

submitted in partial fulfillment of the
requirements for the degree

MASTER OF SCIENCE

Mechanical and Nuclear Engineering
College of Engineering

KANSAS STATE UNIVERSITY
Manhattan, Kansas

2017

Approved by:

Major Professor
Hitesh Bindra

Copyright

Abstract

Storing excess thermal energy in a storage media that can later be extracted during peak-load times is one of the better economical options for nuclear power in future. Thermal energy storage integration with light water-cooled and advanced nuclear power plants is analyzed to assess technical feasibility of different storage media options. Various choices are considered in this study; molten salts, synthetic heat transfer fluids, and packed beds of solid rocks or ceramics. In-depth quantitative assessment of these integration possibilities are then analyzed using exergy analysis and energy density models. The exergy efficiency of thermal energy storage systems is quantified based on second law thermodynamics. The packed bed of solid rocks is identified as one of the only options which can be integrated with upcoming small modular reactors.

Directly storing thermal energy from saturated steam into packed bed of rocks is a very complex physical process due to phase transformation, two phase flow in irregular geometries and percolating irregular condensate flow. In order to examine the integrated physical aspects of this process, the energy transport during direct steam injection and condensation in the dry cold randomly packed bed of spherical alumina particles was experimentally and theoretically studied. This experimental setup ensures controlled condensation process without introducing significant changes in the thermal state or material characteristics of heat sink. Steam fronts at different flow rates were introduced in a cylindrical packed bed and thermal response of the media was observed. The governing heat transfer modes in the media are completely dependent upon the rate of steam injection into the system. A distinct differentiation between the effects of heat conduction and advection in the bed were observed with slower steam injection rates. A phenomenological semi-analytical model is developed for predicting quantitative thermal behavior of the packed bed and understanding physics. The semi-analytical model results are compared with the experimental data for the

validation purposes. The steam condensation process in packed beds is very stable under all circumstances and there is no effect of flow fluctuations on thermal stratification in packed beds. With these experimental and analytical studies, it can be concluded that packed beds have potential for thermal storage applications with steam as heat transfer fluid. The stable stratification and condensation process in packed beds led to design of a novel passive safety heat removal system for advanced boiling water reactors.

Table of Contents

List of Figures

List of Tables

Nomenclature

Symbols

ρ	Density
C	Rate of enthalpy transfer per unit change in temperature
c_p	Specific heat
C_m	Fractional temperature change ratio
e_d	Energy density
f	Vapor phase mass fraction
H	Enthalpy
h	Heat transfer coefficient
k	Thermal conductivity
T	Temperature
t	Time variable
v	Velocity
x	Length variable
$\dot{\mathrm{m}}$	Mass flow rate

Greek Symbols

α	Thermal diffusivity

β Heat transfer coefficient between vessel wall and surroundings

ϵ Porosity or Heat exchanger effectiveness

η Efficiency

λ Latent heat

Ξ Exergy

Dimensionless Quantities

$\Psi = \frac{\rho}{\rho_{in}}$ Dimensionless density

$\tau = \frac{tv}{D}$ Dimensionless time

$\theta = (\frac{T-T_0}{T_{in}-T_0})$ Dimensionless temperature

$\zeta = \frac{v}{v_{in}}$ Dimensionless velocity

$Pe = \frac{Dv}{\alpha}$ Axial Peclet number

$St = \frac{hD}{\epsilon\rho C_p v}$ Stanton number

$X = \frac{x}{D}$ Dimensionless length

Acknowledgments

I would like to thank my advisor, Dr. Hitesh Bindra, for all of the guidance and friendly support he has given me in my research. I am especially grateful for the opportunity he gave me to work with him on the packed bed thermal energy storage analysis.

I also want to thank Dr. Steve Eckels and Dr. Walter McNeil for their time and being apart of my supervisory committee. I am also very thankful to my colleague Dan Gould for sharing his insight and ideas.

I would also like to thank the fellowship support to graduate students by Nuclear Regulatory Commission. I thankfully acknowledge the financial support of National Science Foundation, Department of Energy and State of Kansas for funding the development of this experimental setup and instrumentation capabilities.

Dedication

I would like to dedicate this work to my family. My parents, Barry and Linda, who raised me to be a fine gentleman and taught me the value of an education by their examples. They instilled in me that whatever goal I have I can achieve through hard work and perseverance.

Special thanks go to my brother, Josh, for his continued support. I would not be the person I am today without the examples he set before me to follow and the encouragement he gave me along the way.

Chapter 1

Introduction

Nuclear power plants (NPPs) have negligible carbon emission rates as compared to their fossil fuel counterparts, but their inability to follow grid load demands make them economically less competitive[3;4]. The reason behind this economic disposition for NPPs is because of various associated technical complexities[5;6]. These technical challenges include the adequate handling of reactivity swings caused by time-varying fuel and moderator temperatures, a higher fuel-failure probability due to thermal-structural cycling, and spatial variations in xenon concentrations. Although there are presently some reactors around the world that are operating with flexible load-following capabilities, such operation is restricted to slowly-varying powers, 2-3 times a day, and only up to 80% of the fuel cycle. On the other hand, most of the fossil fueled plants can supply peak-loads by adding more fuel and, thus, can generate far more revenue during those peak hours. The use of NPPs for peak load following is quite complex due to technical constraints associated with reactor behavior. Thus, a more convenient and effective method to facilitate load following by NPPs would be to integrate energy storage. If the grid demand is reduced, then the excess reactor thermal power or plant electrical power is stored in an integrated storage device. This stored energy can be released to the grid when demand is higher than what the NPPs can produce at 100% reactor power[6]. There are many options for storing either the thermal energy from the nuclear reactor or the electricity from the turbo-generator in the power cycle, with both having

their advantages and disadvantages respectively. Thermal, mechanical, and electrical energy storage are the most commonly used storage options. Thermal energy storage is the energy stored in the form of heat in well-insulated solids or liquids, as either sensible heat, stored within a single phase media, or latent heat, stored within phase change materials. Thermal energy storage options include but are not limited to molten salt, packed beds, heating oils, ionic liquids, phase change materials and steam accumulators. Mechanical energy storage is any kinetic or potential energy stored within a device and electrical energy storage resides in the buildup of electrons within systems called electric condensers, which store the charges between two parallel plates when a voltage is applied. Mechanical storage options include but are not limited to compressed air, pumped hydroelectric, flywheels, whereas electrical storage options include batteries and capacitors. Electrical energy storage has the advantage of directly storing the final usable form of energy i.e. electrical energy, but disadvantages come from the high costs and irreversibility. Mechanical energy storage processes such as pumped hydro have higher degree of reversibility but disadvantages include non-negligible energy losses and substantially large space requirements for grid scale storage. Disadvantages with thermal storage is the low efficiency of the conversion process from thermal to electrical energy but with NPPs generating large amounts of thermal heat, a thermal energy storage system becomes advantageous. Therefore, among these various options to store energy, thermal storage is economically more competitive for NPPs as compared to electrical or mechanical storage options.

There have been several studies recently for understanding thermal energy storage systems and their response due to growing energy production from intermittent energy sources, such as solar and wind, and increasing skewedness in the energy demand patterns. Some of the commonly studied thermal energy storage options are; latent heat storage, thermochemical heat storage and sensible heat storage in solid and liquid media. Due to the lower density of gaseous state, the thermal energy storage options are generally limited to solids and liquids. Thermal energy storage (TES) systems although sometimes categorized collectively have diverse set of applications and compatibility challenges with different thermal processes. A TES system for building heating/cooling applications have different design requirements

as compared to TES system for providing dispatchability to power plants. These differences are defined in terms of macroscopic parameters such as exergy efficiency, energy efficiency or energy density. But these are dependent upon detailed thermal behavior or response of the system during storage or recovery processes such as wall effects on energy losses, dispersion and distribution of temperature in TES, or flow-pressure behavior[7;8]. These detailed thermal responses are directly effected by the choice, size or shape of the storage material and the system involved. They are also dependent upon the heat transfer fluid (HTF), operating pressure-temperature conditions, modes of interaction – direct/indirect or natural/forced circulation and flow rates. In most of these cases with different paired sets of HTF and TES media, a detailed model and experimental set-up for validation is designed to evaluate the potential for TES system with spatio-temporal detailed characteristics. Recently there have been studies[9;10] where such detailed thermal behavior of the storage systems were studied during storage or recovery processes. These studies have been performed for solid as well as liquid storage media, and sensible heat or latent heat type of TES. But in all of these studies the heat carrier or HTF was in a single phase – i.e. gas or liquid state for all scenarios.

One distinct class of sensible heat TES solutions is packed bed of solids, which has been one of the prime candidates for storing energy for various applications. The randomly packed beds of gravel, alumina or ceramics, due to their high energy density, low cost, high reversibility and high exergy efficiency make them one of the top candidates for energy storage option and have been tested with air, gases and liquid type HTFs. Packed bed TES designs are not only limited to sensible heat storing solid rocks but also include phase-change materials, filled small to large size encapsulating balls. The physical design and assembly of such systems is very simple but their design suitability is highly dependent upon the temperature distribution which is very sensitive to thermal properties and operating parameters. Thus, high fidelity of understanding with detailed mathematical models is essential to design the optimum system[11–14].

The next chapter will focus on the topic of exergy efficiency evaluation on TES options for integration with NPPs. The exergy efficiency of TES systems is quantified based on second law thermodynamics. In Chapter 3, the packed bed of solid rocks is identified as one

of the only options which can be integrated with upcoming small modular reactors. Chapter 4 provides the experimental work on investigation of the heat transfer between the solid particles and condensing steam during experiments with steam injection in packed bed of alumina particles. Chapter 5 details the novel idea of the packed bed system as a passive safety heat removal system with steam for boiling water reactors, and then conclusions over the work are made in Chapter 6.

Chapter 2

Sensible heat storage integration

2.1 Introduction

The adoption of a particular thermal storage option is largely dependent upon the operating and process conditions of the nuclear heat source and reactor coolant. Light water-cooled NPPs operate at lower temperatures than Next Generation Nuclear Power (NGNP) reactors and only use pressurized water as the main coolant, whereas NGNP reactors use molten salts or high temperature gasses as the main coolant. The critical step remains how to select and develop an ideal choice of heat transfer fluid or storage media[7]. Currently, there are some thermal storage solutions such as molten nitrate salt, also known as storage or solar salt ($40\%KNO_3 + 60\%NaNO_3$) and packed bed of alumina particles which present very low technological risk and a high deployment potential. These solutions can be good candidates for some of the advanced high-temperature reactors but have some limitations for integration into light water-cooled NPPs. Therefore, other materials such as synthetic heat transfer fluids need to be explored to evaluate the options to store thermal energy for light water-cooled NPPs. An overall comparative economic analysis can help in decision making process for storage integration, but for new materials and methods it is difficult to estimate the actual costs or effective costs if those technologies are deployed in large scale. An energy density and exergy model are used to compare different technologies and materials in this

study.

2.2 Nuclear Power Plants considered

Firstly, different NPPs which can be considered as potential candidates for TES integration will be briefly described with sufficient details in the process system conditions. For this analysis three NPP designs are selected - light water-cooled small modular reactors (LW-SMR), the modular high-temperature gas-cooled reactor (MHTGR) and pebble-bed fluoride-salt-cooled high-temperature reactor (PB-FHR). The schematics of each type are shown in Figures 2.1-2.3, and Table 2.1 shows key features of the different reactor systems. The basis of selection of these designs is to analyze a broader spectrum of reactor operation temperatures and to understand the impact of substantially different thermo-physical properties of the reactor coolant. The mode of thermal storage integration is however kept similar in all possible combination of NPPs and TES systems.

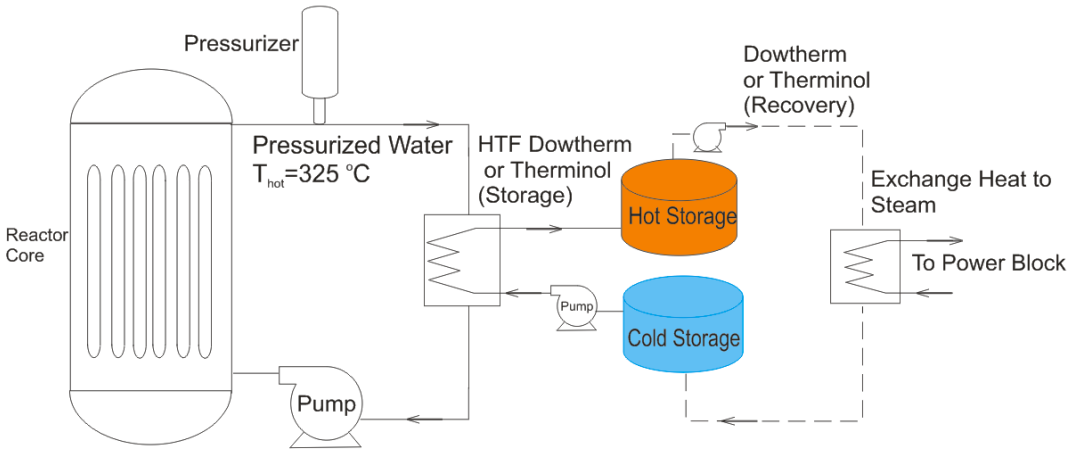

Figure 2.1: *Light water-cooled small modular reactor integrated with a two storage tank system with either therminol or dowtherm as storage medium.*

2.2.1 Light Water-Cooled NPPs

Light Water-cooled Reactors (LWRs) produce saturated steam to operate steam turbines on the Rankine cycle principles and are the most widely established type of NPPs throughout

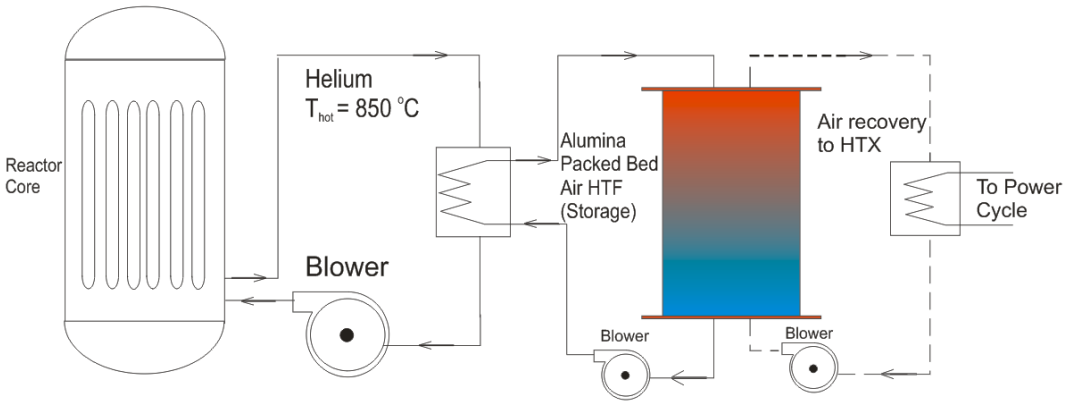

Figure 2.2: *Modular high-temperature gas-cooled reactor integrated with a packed bed storage system with alumina spheres as the packing material.*

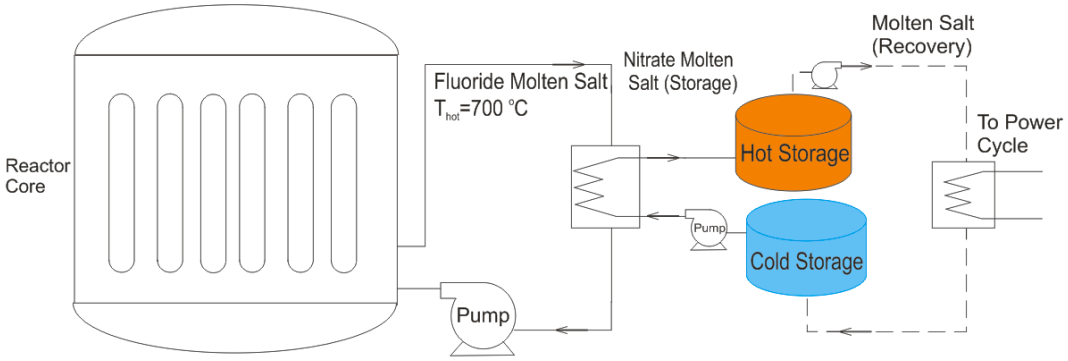

Figure 2.3: *Pebble bed fluoride-salt-cooled high-temperature reactor integrated with a two tank storage system with molten nitrate molten salt as storage medium.*

the world. LWRs are further categorized as Boiling-Water Reactors (BWRs), Pressurized-Water Reactors (PWRs) and LW-SMRs (Light water-cooled small modular reactors). BWRs produce steam directly through core heat transfer and require more attention to ensure safety of thermal storage and will not be considered in this study. PWRs consists of the nuclear reactor where pressurized light water is circulated to remove the reactor heat and transfer it to a secondary side, via steam generator that transfers the thermal energy of the pressurized water to produce steam that runs through the turbine in the outer Rankine cycle loop. On the other hand, BWRs do not have two loops and the reactor coolant i.e. light water gets directly converted into steam which is then used as a working fluid to do mechanical work. There are small modular designs for both PWRs and BWRs, which are categorized as LW-SMRs. Due to thermodynamic and heat transfer limitations, both types of the LWRs

produce steam at $280°C$ or less. At these temperatures thermodynamic efficiency is close to 35%, therefore integrating thermal energy storage must not deteriorate the exergy efficiency further. The two routes of storing heat energy in LWR plants are - directly storing the energy from working fluid i.e. steam, or extracting thermal energy from primary coolant into energy storage media. Due to latent heat of steam, the direct heat recovery from steam into storage media is associated with pinch point. Therefore BWRs are naturally in a disadvantageous position for thermal storage integration as compared to PWRs. In the PWRs, the losses due to heat transfer between the pressurized water and steam is one of the significant reasons for the exergy destruction. Therefore ideal configuration for storage integration is to store the energy from the primary reactor coolant i.e. pressurized light water. However, in NPPs the reactor coolant (RC) is considered as one of the intermediary layers for radioactivity containment, so for safety measures the coolant is generally not allowed to leave the containment building. This safety philosophy and large volume requirements for TES systems, postulate the thermal storage integration to NPPs via heat exchange between RC and secondary HTF. Thus for nuclear safety requirements the heat exchanger which exchanges heat between RC and HTF can be housed inside the reactor containment building. The hot HTF is brought outside the reactor containment building to store energy in a TES system. Nevertheless, the secondary reason for the need of this heat exchange process arises due to the compatibility issues of different TES systems and HTF requirements. In case of existing NPPs, the reactor containment building layout generally does not have enough flexibility to add additional heat exchange equipment of large scale. But in the new light water-cooled NPP designs such as LW-SMRs, this design provision in the reactor building layout can be made.

Due to the presence of additional resistances in the heat exchanger, the actual storage inlet temperature T_{in} is lower than the RC outlet temperature and thus is dependent upon the effectiveness of an indirect heat exchange process or design. Irrespective of the design details of heat exchange equipment, the heat transfer between two streams can be solved using the effectiveness values to obtain the HTF temperature during storage cycles. The operating temperatures and RC properties are provided in Table 2.2 for the LW-SMR [15].

2.2.2 Advanced NPPs with advanced coolants

In recent years the focus for new nuclear power plants has been on higher operating temperatures to improve overall plant efficiency and increase the outlet temperature of the main coolant. Increasing the outlet temperature allows for other possible applications such as hydrogen production or petroleum refining, in addition to higher efficiency power cycles. The performance of thermal energy storage options is also highly dependent upon temperature, as concluded by many previous studies[8;11;16–18].

Modular High-Temperature Gas-Cooled Reactor

MHTGRs utilize helium for the RC flowing through a graphite moderated core, where the outlet temperature of helium can reach temperatures of 1000 °C and higher, leading to higher thermal-to-electrical energy efficiency than that of light water-cooled NPPs, using an intermediate heat exchanger coupled with a helium-brayton cycle. Helium also has advantage of being a safer RC over water due to no threat of film boiling or two phase flow causing a reactor accident. In this study the focus is on a prismatic bed MHTGR design that has a electrical output of 286 MW(e) and the reactor system is rated at 600 MW(th). The operating conditions and RC properties at the average temperature are listed in Table 2.2 for the MHTGR[19]. Similar to LW-SMRs described before, the philosophy of safety requires a secondary HTF to transfer thermal energy from RC to a TES system located outside the containment. In case of gas-cooled reactors, one of the major apparent difference is in the higher temperature differences between inlet and outlet conditions. This is attributed to lower density as compared to liquid coolants leading to relatively smaller energy carrying capacity. Due to higher temperature differences, if the effectiveness of heat exchange process between RC and HTF is poor it leads to proportionate losses thereby resulting in larger differences between the reactor outlet temperature and storage inlet temperature. Thus, the impact of heat exchange process effectiveness must be investigated more carefully for MHTGRs.

Table 2.1: *Key features for the three discussed reactor types.*

NPP type	LW-SMR[15]	MHTGR[19]	PB-FHR[20]
Reactor Coolant	Water	Helium	FLiBe
Working Fluid	Steam	Helium	Air
Reactor Thermal Power (MW_{th})	500	600	236
NPP electric output (MW_e)	158	286	100

Pebble-Bed Fluoride-Salt-Cooled High-Temperature Reactor

PB-FHR design has fluoride molten salt (FLiBe) as the RC with fuel and reflector in the shape of spherical pebbles. The molten salt circulates through the pebble bed core and obtains the core outlet temperature of 700 °C before exchanging its thermal energy to secondary cycle for power production, or a secondary molten salt coolant for other high temperature processes, such as hydrogen production. Molten salt as the RC has advantages of no high pressure requirements or gas-liquid two phase interfaces, and it also allows high temperature operation as compared to LWRs. Due to low vapor pressure at higher temperatures, it remains in liquid state at atmospheric pressure. The PB-FHR design is a 236 MW(th) reactor system, with a corresponding electrical power rating of 100 MW(e) at the base-load operation. Operating conditions and RC properties are provided in Table 2.2 for the PB-FHR[20]. Similar to design philosophy of the two reactors described above, all the RC system components remain within the containment and TES layout will be outside the reactor building. So the goal is to find a compatible HTF which can remove the heat effectively from the molten salt.

2.3 Thermal Energy Storage Options

Sensible TES is more robust and established than any other thermal energy storage system[18;21]. It has been shown by Bindra et al.[22] that sensible heat storage have much higher

Table 2.2: *Thermal properties for Nuclear Power Plants reactor coolants for the three discussed reactor types.*

NPP type	LW-SMR[15]	MHTGR[19]	PB-FHR[20]
Reactor Coolant	Water	Helium	FLiBe
Inlet/Outlet Temp. (^oC)	290/325	490/850	600/700
Density (kg/m^3)	900	2.7902	1889.15
Specific Heat (kJ/kg-K)	6	5.1903	2.4
Thermal conductivity (W/m-K)	0.0468	0.413	1
Viscosity (mPa-s)	1	0.0526	7.524

exergy efficiency for high energy density storage design as compared to other mechanisms. So, in this work integration studies are only performed with sensible TES. The temperature difference between cold state and hot state, and thermal capacity of the media determine energy density of sensible heat. Solid and liquid sensible heat storage solutions are most common and both offer advantages and disadvantages for storing thermal energy at different operating temperatures. Solids have higher energy density but can make the design and integration complicated due to the need of a tertiary heat transfer fluid. Liquids such as molten salt don't need a tertiary media as they have sufficient thermal capacity to be stored 'as it is' when they are hot without any pressurization requirements. However, liquid options can have more operating constraints which limit their operating range such as, most of the molten salts can not be used for light water-cooled NPPs because of their higher melting temperature, i.e. 200 °C or above. This temperature constraint compels the system to have an auxiliary heating mechanism such as electrical heating to ensure the molten salts remain in molten state even when the NPP is not operating or when not storing heat. Thus, an overall technical feasibility analysis must be conducted in selecting the type of TES system.

2.3.1 Various TES technologies

TES solutions which are discussed in this work are the well established materials and methods - storage salt ($40\%KNO_3 + 60\%NaNO_3$) two-tank storage, synthetic heat transfer fluids in two-tank storage configuration, and solid alumina particles in packed beds. Storage salt (nitrate) is popularly known as solar salt or molten salt, but in this work in order to avoid confusion FLiBe will be the only salt referred to as molten salt. Figure 2.4 shows the NPP types integrated with the TES storage media options investigated in this study. The storage or secondary heat transfer fluid temperature in a nuclear energy system is limited to the temperature of the RC. There are two categories of secondary or storage media HTFs for NPPs: gaseous heat transfer fluids such as air or CO_2, and storage salt or any other high temperature liquid. Gaseous phase heat transfer fluids, due to their low density and thus lower thermal capacity, act as a tertiary media for transferring heat from the primary system to solid thermal energy storage which has much higher thermal energy density. The temperature difference between the cold state and hot state of the liquid determines the energy density. As mentioned earlier, storage salts because of their higher melting temperature, i.e. 200 °C cannot be used for LWRs such as SM-LWRs which require the system to have auxiliary heating mechanism such as electrical heating to ensure the molten salts will remain in molten state even when the NPP is not operating. This auxiliary heating system will lead to higher parasitic losses and can lead to lower efficiency for LWRs. Thus, the alternative ideal fluid to transfer and store this thermal energy should be a liquid near the RC temperature at atmospheric pressure, has a melting point below the room temperature, has sufficient thermal capacity and is also stable up to the operating reactor temperature. The only types of fluids which satisfy all these criteria and pose low technological risk are synthetic HTFs such as Therminol66 (modified terphenyl) or DowthermT (mixture of $C_{14} - C_{30}$ alkyl benzenes). However, these operating temperature challenges do not play any significant role for advanced reactor designs which have primary system at much higher temperatures as compared to melting temperature of storage salts. Therefore advantages and challenges of different thermal storage media should be evaluated based on overall performance of the

Table 2.3: *Thermal properties for Therminol and Dowtherm (at average temperatures for energy storage i.e. 570 K)*

Storage type	Therminol66[23]	DowthermT[24]
Density (kg/m^3)	816	687
Specific heat (kJ/kg-K)	2.531	2.767
Thermal conductivity (W/m-K)	0.096	0.075
Viscosity (mPa-s)	0.44	0.39
Min. operating Temp. (K)	270	263
Max. operating Temp. (K)	588	618

integrated system. The comparison of thermal storage media properties for low temperature and high temperature integration are reported in Table 2.3 and Table 2.4, respectively. The concept design for the various TES integrated options for the NPP types and TES types can be seen in Figures 2.1-2.3. Figure 2.1 is of an LWR integrated with the two storage tank option for either Therminol or Dowtherm as the storage media. Figure 2.2 shows a MHTGR integrated with a single alumina packed bed storage system utilizing air as the HTF, and Figure 2.3 has a PB-FHR integrated with a two storage tank system for Solar salt as the storage media.

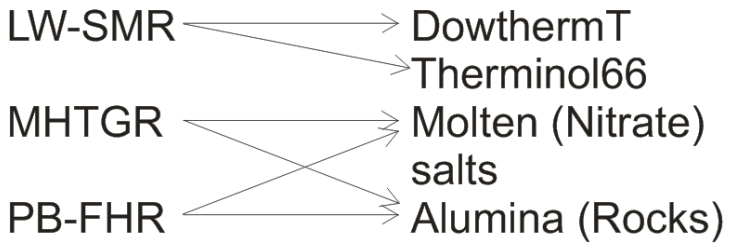

Figure 2.4: *NPPs matched with potential TES options*

Table 2.4: *Thermal properties for Solar salt and Alumina (at average temperatures for energy storage i.e. 900 K)*

Storage type	Solar Salt[25]	Denstone-99 Alumina[26]
Density (kg/m^3)	1790	3930
Specific heat (kJ/kg-K)	1.560	1.195
Thermal conductivity (W/m-K)	0.51-0.60	9.685
Viscosity (mPa-s)	1.3-1.6	NA
Melting point (K)	415	NA
Max. operating Temp. (K)	1000	NA

2.4 Exergy and Energy density quantification model

The disadvantage of the heat transfer in the heat exchanger between the RC and HTF for storage is that it reduces the maximum temperature during storage and in turn exergy efficiency of the system. The heat exchange process between HTF and RC is an important component of the model which involves indirect heat exchange to the HTF of the TES system. Due to the presence of additional resistances in the heat exchanger, the actual storage inlet temperature T_{in} is lower than the RC outlet temperature and thus is dependent upon the effectiveness of an indirect heat exchange process or design. Irrespective of the design details of heat exchange equipment, the heat transfer between two streams can be solved knowing an effectiveness for the heat exchanger to obtain the HTF temperature. The generic heat transfer model can be written as,

$$(T_{RC} - T_{HTF}) = f(\epsilon, \dot{m}) \tag{2.1}$$

where, T_{RC} is RC temperature, T_{HTF} is HTF inlet temperature to TES, ϵ is the overall heat transfer effectiveness in the heat exchange process, and $\dot{m}$ is the coolant flow rate.

For present study of system exergy quantification, the following assumptions can simplify

the analysis: a) the temperature difference between the RC and HTF streams remains constant throughout the flow path inside the heat exchanger, and b) the overall heat transfer coefficient is only dependent upon the minimum heat transfer coefficient across the heat exchange equipment. Based on these assumptions, inlet temperature for energy storage can be estimated. Therefore, introduction of thermal storage reduces the temperature at which energy is produced. Thus storage leads to exergy destruction due to heat transfer resistance. The effect of exergy reduction due to reduction in temperature of energy transfer reduces the exergy ultimately going to the power block.

2.4.1 HTF Temperature

In this problem both inlet and outlet temperatures of RC are fixed as they govern reactor behavior directly and any changes in that will involve serious considerations for reactor safety and regulatory aspects. Using these fixed RC inlet and outlet temperatures, the inlet and outlet temperatures of HTF can be evaluated using standard heat exchanger design equations. Rate of enthalpy transfer per unit change in the temperature labeled as C_r and C_f, are used to compute the fractional temperature change ratio C_m, i.e. the ratio of change in temperature of the minimum enthalpy fluid to maximum enthalpy fluid (Equations 2.2-2.4).

$$C_r = \dot{m}_r c_{p_r} \tag{2.2}$$

$$C_f = \dot{m}_f c_{p_f} \tag{2.3}$$

$$C_m = \frac{C_r}{C_f} \tag{2.4}$$

The subscript 'r' denotes hot side fluid i.e. RC and 'f' denotes cold side fluid i.e. storage HTF. So first the effect of this heat exchange process is modeled and then the HTF temperature is obtained for the storage inlet condition. With the assumption that temperature

differences remain constant between the RC and HTF and using the fractional temperature change ratio and setting an effectiveness for the heat exchanger depending on the RC and HTF, the HTF outlet temperature is calculated using equations 2.5-2.7.

$$\Delta T_f = C_m \Delta T_r \tag{2.5}$$

$$T_{f,in} = T_{r,in} - \frac{\Delta T_f}{\epsilon} \tag{2.6}$$

$$T_{f,out} = T_{f,in} + \Delta T_f \tag{2.7}$$

It should be noted that if effectiveness, ϵ, is not known, NTU must be known to compute the effectiveness for a particular heat exchange process. In this work the range of effectiveness is selected based on temperature data in the primary and secondary side across heat exchangers.

2.4.2 Exergy modeling

Exergy efficiency is an effective indicator to find the actual value of TES integration in power plants. Extensive work on exergy analysis of TES systems has been performed for the storage and recovery stages of the TES cycle[22]. From this previous work the exergy of the inlet fluid/gas storing the thermal energy in a TES system is given by

$$\Xi_{st} = \int_{t_p} \{\dot{m} C_{pf} (T_{r,in} - T_0) - \dot{m} C_{pf} T_0 ln(\frac{T_{in}}{T_0})\} dt \tag{2.8}$$

where, C_{pf} is the specific heat of fluid and T is the temperature. The exergy is stored in the TES unit for a time period (t_p), where it is then recovered and the exergy of the outlet fluid is equal to

$$\Xi_{re} = \int_{t_p} \{\dot{m} C_{pf} (T_{f,out} - T_0) - \dot{m} C_{pf} T_0 ln(\frac{T_{out}}{T_0})\} dt \tag{2.9}$$

The subscripts 'in,' 'out,' and '0' represent 'inlet,' 'outlet,' and 'reference' conditions respectively. The fractional exergy recovery or exergy efficiency of the storage system is computed for evaluating the economics. The basic model of converting dynamic temperature output information from storage system to exergy parameters has been detailed previously[27].

$$\eta_{th} = \frac{\Xi_{re}}{\Xi_{st}} \tag{2.10}$$

Dimensionless temperature, $\theta = \frac{T_f - T_0}{T_r - T_0}$, is used to simplify the exergy calculations to

$$\eta_{ex} = \frac{\int_{t_p}[\theta + \frac{1-\eta_{carnot}}{\eta_{carnot}} ln(\theta_f(\frac{\eta_{carnot}}{1-\eta_{carnot}} + 1)]dt}{\int_{t_p}[1 + \frac{1-\eta_{carnot}}{\eta_{carnot}} ln(\frac{1}{1-\eta_{carnot}})]dt} \tag{2.11}$$

where, η_{carnot} is the Carnot efficiency based on reference temperature, T_0 and outlet temperature of RC, T_r. The electrical energy density is dependent upon exergy efficiency of thermal storage system which is in turn dependent upon temperature of reactor operation and heat exchanger performance.

2.4.3 Packed bed of solid rocks

As mentioned before, high temperature solids such as alumina or gravel are good candidates to store energy at very high temperatures (beyond the operating range of RC temperatures). However, they need a tertiary HTF to transfer heat from the RC. Therefore, modeling heat transfer between tertiary HTF and the TES(solids) involves an additional step[28], thus an energy balance must be solved numerically to find the temperature of air exiting the packed bed during recovery. This model can be written as set of two coupled differential equations (2.12 and 2.13) and has been presented in detail in a previous work[22].

$$\frac{\partial}{\partial t}(\rho_f C_{pf} T_f) + v\frac{\partial}{\partial x}(\rho_f C_{pf} T_f) = \frac{\partial}{\partial x}[k_f \frac{\partial T_f}{\partial x}] - h_{fs}(T_f - T_s) - \beta_w(T_f - T_0) \tag{2.12}$$

$$\frac{\partial}{\partial t}(\rho_s C_{ps} T_s) = \frac{\partial}{\partial x}[k_f \frac{\partial T_f}{\partial x}] + h_{fs}(T_f - T_s) \tag{2.13}$$

where, k is thermal conductivity, h_{fs} is fluid-solid volumetric heat transfer coefficient and β_w is the wall heat transfer coefficient. The boundary and initial conditions for this packed bed model can be described for storage and recovery cycles independently. In the storage cycle, hot HTF from heat exchanger enters from the one end and during the recovery cycle HTF enters at ambient temperature from the other end. More details on the model descriptions can be obtained from previous references[22;27]. The outlet temperature of HTF during the recovery cycle is then used to compute the exergy as described in the Eqn. 2.11.

2.4.4 Energy density

In case of thermal storage, the costs are directly related to the ability of recovered heat to provide useful work. Thus an exergy model which takes into account thermal energy losses, additional work requirement and entropy generation due to mixing or dispersion effects will be developed. Based on the reactor operation temperature, both the cycle efficiency and exergy efficiency of the storage system can be determined as explained before. If total thermal energy density of the storage system is known it can be used to compute electricity units stored per mass of storage material.

$$e_{d,th} = C_p(T_{c,out} - T_{amb}) \tag{2.14}$$

where $e_{d,th}$ is the thermal energy density and T_{amb} is the ambient temperature. In case of storage salt the lowest possible temperature is its melting point, T_{mp} which replaces T_{amb} for the TES density calculations, which would dramatically reduce their energy density for existing nuclear power plants. It should be noted that T_{amb} is used considering that storage HTF will first derive energy to be stored from feed-water loop starting from condenser outlet (close to $20°C$). Thermal energy density can be converted to effective energy density using,

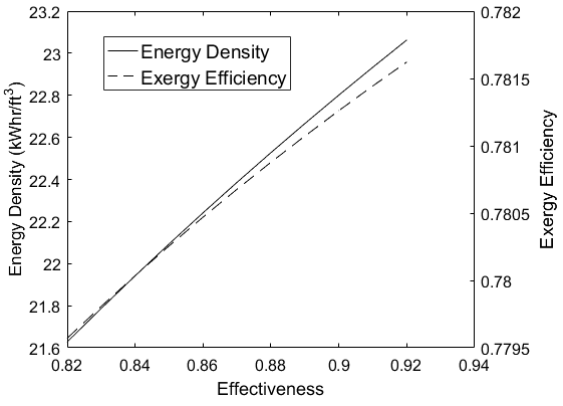

Figure 2.5: *MHTGR integrated with alumina packed bed storage.*

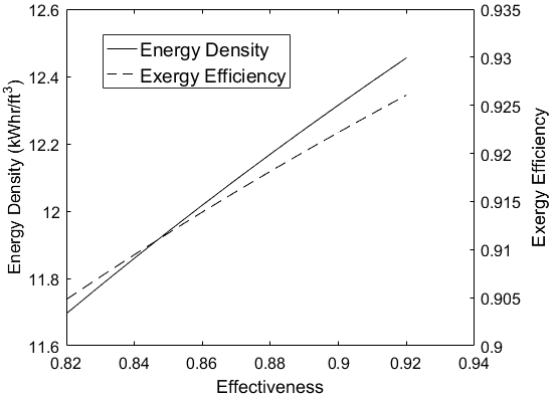

Figure 2.6: *MHTGR integrated with nitrate molten salt storage.*

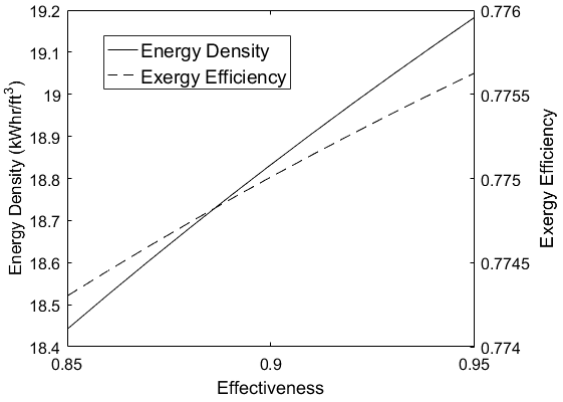

Figure 2.7: *PB-FHR integrated with alumina packed bed storage.*

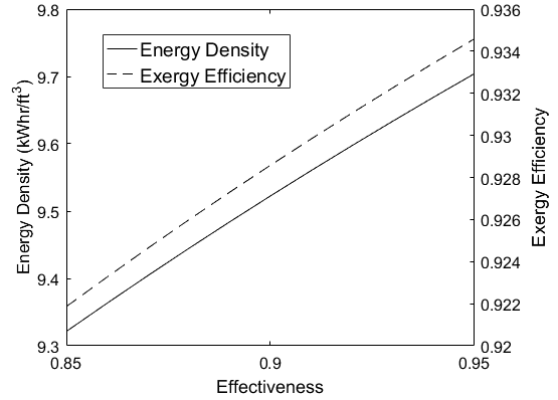

Figure 2.8: *PB-FHR integrated with nitrate molten salt storage.*

$$e_d = e_{d,th}\eta_{exer} \tag{2.15}$$

where, e_d is the effective thermal energy density based on exergy efficiency.

2.5 Results

This study evaluates the exegetic performance of different materials and methods to store thermal energy of NPPs. The analysis was conducted for thermal storage integration with existing and future generation NPPs based on the plant design data from literature[15;19;20].

Table 2.5: *Effectiveness and C_r values for the varying RC and HTF proposed combinations.*

NPP/TES combination	Effectiveness (ϵ)	C_m
LW-SMR/Therminol	0.92	1
LW-SMR/Dowtherm	0.92	1
MHTGR/Nitrate Molten Salt	0.89	0.5
MHTGR/Air-Alumina	0.82	1
PB-FHR/Nitrate Molten Salt	0.92	1
PB-FHR/Air-Alumina	0.85	2

The study reveals that there are various possible options to store thermal energy of next generation NPPs efficiently, but the options for existing NPPs are limited. Low technological risk sensible heat storage materials such as molten salt, concrete or alumina can be beneficial for high temperature NPPs. Development of new materials such as ionic liquids might be required for making storage integration to existing NPPs feasible. The values for the effectiveness along with the C_r values were set depending on the RC and HTF being integrated together. These values are given in Table 2.5 and the resulting exergetic efficiency of liquid thermal storage is 92-93%, while solid thermal storage is 77-78% if integrated with NPPs, as seen in Table 2.6.

The numerical values of storage inlet, outlet, exergy efficiency and energy density are computed based on the method and model presented in previous sections along with the thermal properties for Therminol-66 and Dowtherm-T listed in Table 2.3 and storage salt and Denstone-99 alumina listed in Table 2.4. The numerical results presented in Table 2.6 show that Therminol has equivalent exergy recovery but has slightly higher energy density for the lower temperature reactors. While for higher temperature reactors the nitrate molten salt storage media has higher exergy efficiencies but the alumina packed bed storage has higher energy density. As the energy costs are directly related to these functions, Therminol

Table 2.6: *Performance of different thermal storage technologies integrated with corresponding NPPs, detailed earlier in the chapter. Temperatures are given in Kelvin and energy density e_d in $kWhr/ft^3$.*

Storage type	T_{Cin}	T_{Cout}	η_{ex}	e_d
Storage Salt				
MHTGR	647.75	827.8	0.9202	12.462
PB-FHR	591.3	691.3	0.9311	9.5974
Alumina (Air HTF)				
MHTGR	410.98	771	0.7684	22.3536
PB-FHR	464.71	664.71	0.7857	18.4419
Therminol				
LW-SMR	286.96	321.96	0.9349	4.815
Dowtherm				
LW-SMR	286.96	321.96	0.9349	4.44

will perform better economically and thermodynamically for LW-SMRs and for the MHTGR or PB-FHR, nitrate molten salt results in higher outlet temperatures, leading to the higher exergy efficiency and overall energy stored and recovered in the system.

2.6 Summary

This chapter provides a conceptual presentation on the integration of NPPs with technically robust thermal energy storage solutions. The conceptual presentation is based on energy density and exergy analysis. Therminol and Dowtherm are commercially available robust technological solutions for this purpose and operate in the temperature range highly compatible with the existing PWRs and upcoming LW-SMRs. Whereas Alumina and Storage

salt are more suitable for high-temperature NGNPs.

The analysis for lower temperature reactors shows that exergy recovery efficiency is around 90% and energy density values for the synthetic HTFs in this operating range are not expected to create practical challenges. The high temperature storage options, alumina packed beds and storage salt show exergy efficiency of 78% and 92%, respectively. The overall exergy efficiency and energy density can be improved with higher heat exchanger effectiveness as shown in Figures 2.5-2.8. The liquid-type TES solutions show much higher thermal exergy efficiency as compared to solids, as presented in Table 2.6. It is anticipated that Alumina and Storage salt will consume non-trivial fraction of energy stored to compensate for losses such as auxiliary heating or pressure drop, but these are largely dependent upon plant layout, and details will be possible only with fixed details on plant layout. Nevertheless, the exergy analysis presented in this work will be useful for future economic analyses if the costs of storage materials are available at large scale. Further, TES integration will require heat exchange between RC and HTF, i.e. it will add equipment or physical boundary from where RC can potentially leak or escape. Therefore, the layout of the plant can impose restrictions in the implementation of these integration concepts. Next chapter discusses more advanced concept which can be applicable for upcoming nuclear power plants.

Chapter 3

Packed bed thermal storage for LW-SMRs

3.1 Introduction

The previous chapter developed models and performed exergy analysis for integrating sensible heat type TES with LWRs and SMRs[29;30]. These exergy based models show that technical feasibility index of integrating thermal energy storage is very high. But most of these previous studies, shown in Chapter 2, include integration based on existing layout of NPPs with heat exchange between storage HTF and RC. However, most of the LW-SMR based NPP designs can not accommodate additional heat exchange equipment, such as shown in Figure 3.1 where volume of reactor containment for a standard 1000 MWe NPP is compared to NuScale 50 MWe[1]. Although power production is only reduced to 1/20th scale, the containment volume in the NuScale LW-SMR is reduced to $\sim$ 1/170th scale. As steam is the secondary or working fluid which exits out of the reactor containment in LW-SMRs, the simplest and most practical way to integrate thermal storage with LW-SMRs is to directly store the energy from steam. Indirect heat exchange between steam and another heat transfer fluid during the storage process, and then heat recovery again via indirect heat exchange is inefficient process due to heat transfer resistance. This inefficiency is due to what is called

as 'pinch point' which occurs whenever there is indirect heat transfer between two media where one undergoes phase change and other undergoes change in sensible heat. Another existing popular option is to use a steam accumulator which stores dry or wet steam directly inside the pressure vessels, however, due to large volumetric requirements it is not a viable option.

Previously, packed bed type thermal energy storage systems have been invented and optimized to work for single phase heat transfer fluids[31;32]. This work proposes the modification of those designs, where steam produced in the secondary side of LW-SMRs can be injected into the packed bed of inert particles with sufficient thermal conductivity and capacity to efficiently store energy with high energy density.

With the integration of this system, the changes in the load demand will not effect the LW-SMR operation and the excess steam will be diverted to TES. When the demand increases this stored energy in hot packed beds can be recovered by injecting cold pressurized water. Although there are some existing packed bed TES models which use single phase HTFs, these models have not been extended for steam as the HTF i.e. essential for this proposed integration[22;27].

This thermal model is extended to assess behavior of packed bed TES system under storage and recovery cycles. Steam is the only HTF which exits the reactor vessel, so any application such as process heat or TES integration should be evaluated with steam as process fluid. This project will develop a process system integration model of LW-SMR with packed bed type TES using steam as HTF.

3.2 Physical description of the system

A typical packed bed TES system consists of fluid path, storage vessel internally lined with refractory or insulating material and packing material. If the HTF undergoes phase change, as in this case, it is required that density changes do not produce any significant thermal ratcheting. In previous studies of steam testing with Alumina, it has been confirmed that Alumina rocks of 3-6 mm particle size, do not exhibit any ratcheting under thermal cycles.

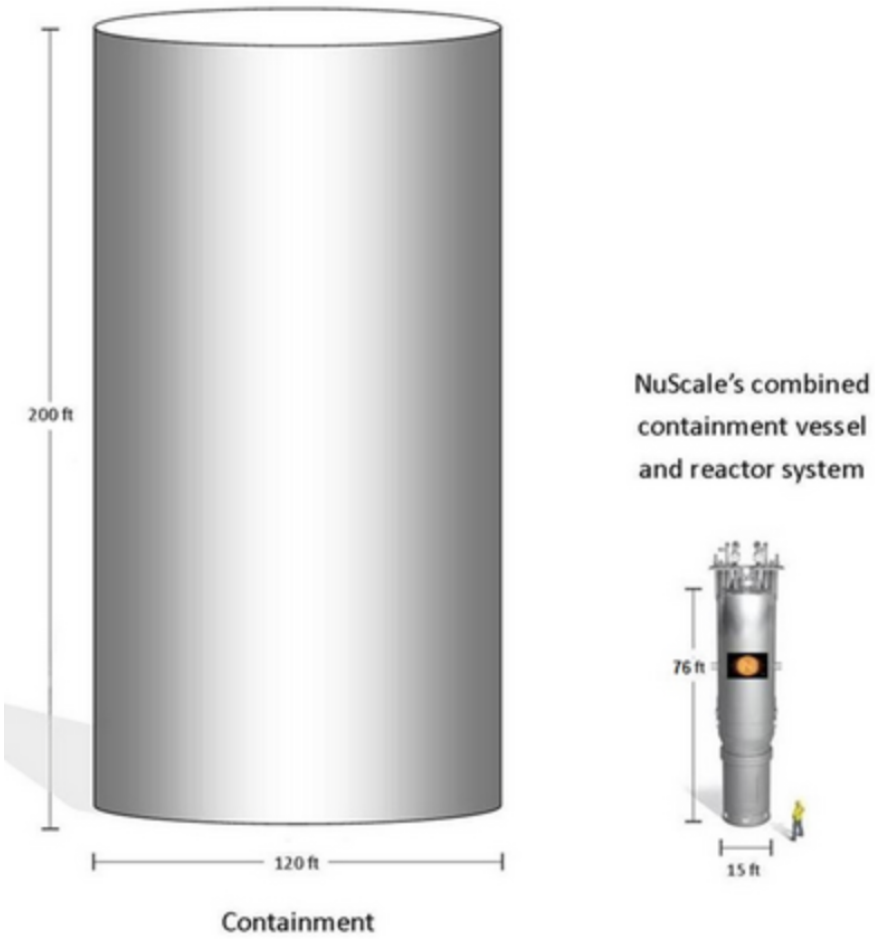

Figure 3.1: *Reactor containment size comparison between existing LWRs and LW-SMRs (NuScale[1])*

Other advantages of Alumina particles are their higher thermal capacity and higher thermal conductivity. In the following section, a detailed description of theoretical model is provided.

3.3 Model description

A theoretical evaluation of the heat storage and recovery process that employs steam as the carrier fluid and bed of alumina particles as storage media is accomplished through the development of three-phase (solid-liquid-vapor) mathematical model. The model is based on a homogeneous mixture of two phases during a phase change (boiling/condensation). The remaining part of the model is exactly same as the two-equation model used for the single phase gas/solid heat transfer model described earlier in the previous chapter. The basic assumptions for this model are – **(a)** There are no pressure changes accompanied by phase change phenomenon. **(b)** There is no temperature gradient inside the particles; this is based on low velocities and a high thermal conductivity within the particles (as is our case). In this base case, where the fluid velocity is 0.1 m/s and the alumina particle size is 3 mm, the assumption is valid. Higher velocities and higher particle sizes can lead to violation of this assumption; this means that the temperature inside the particles cannot be considered uniform and this is not suitable for storage system as it causes spreading of the thermal front. **(c)** No dispersion occurs in the vapor phase due to thermal conduction. At sufficiently low velocities thermal dispersion is negligible. In addition, when the robustness of the system is to be tested, thermal dispersion models are applicable when system behaves in an ideal manner. **(d)** Latent heat can be approximated with specific heat over a temperature differential of 1°C. The higher the δT selected, the lower the accuracy but the numerical complexity decreases. **(e)** During phase change, the liquid-vapor phase forms a homogeneous mixture with no stratification.

The model only considers energy and mass conservation equations for the fluid phase as shown by Eqn. 3.1 and Eqn. 3.2 respectively.

$$\frac{\partial \rho}{\partial t} + \frac{\partial \rho v}{\partial x} = 0 \tag{3.1}$$

$$\frac{\partial \epsilon \rho H}{\partial t} + \frac{\partial \epsilon \rho H v}{\partial x} = -h(T - T_s) \tag{3.2}$$

However, as the solid media mass remains as constant, only energy conservation is modeled for solid media.

$$(1 - \epsilon)\rho_s C_{ps} \frac{\partial T_s}{\partial t} = h(T - T_s) \tag{3.3}$$

Solid enthalpy can be related to the reference temperature directly, whereas enthalpy of the fluid phase can be expressed as

$$H = C_{pl}(T_{sat} - T_{ref}) + f\lambda_{lg} + C_{pg}(T - T_{sat}) \tag{3.4}$$

The phase change term $f\lambda_{lg}$ can be converted to a simplified sensible heat approximation (sharp temperature jump around phase change temperature).

$$H = C_{pl}(T^I_{sat} - T_{ref}) + C_{p,jump}(T^{II}_{sat} - T^I_{sat}) + C_{pg}(T - T^{II}_{sat}) \tag{3.5}$$

Density of fluid phase can be described as,

$$\rho = \rho_g + (1 - f)\rho_{lg} \tag{3.6}$$

which can be approximated to

$$\rho_f = \rho_g + (1 - (\frac{T - T_{sat}}{T_{sat} - T^I_{sat}})) + \rho_{lg} \quad \textbf{if } T^{II}_{sat} > T > T^I_{sat} \tag{3.7}$$

Enthalpy jump approximation can be explicitly stated as,

$$C_{p,jump}(T^{II}_{sat} - T^I_{sat}) = (f^{II} - f^I)\lambda_{lg} \tag{3.8}$$

$$f^{II} = 1 \quad f^{I} = 0 \tag{3.9}$$

Non-dimensionalized form of these equations can be converted to the following set, using the dimensionless parameters listed in Nomenclature.

For $\theta > \theta^{II}_{sat}$

$$\Psi\zeta = 1 \qquad \text{(Continuity)}$$

$$\frac{\partial\theta_g}{\partial\tau} + \frac{\partial\theta_g}{\partial X} = -St_g(\theta_g - \theta_s) \qquad \text{(Energy)}$$

$$\frac{\partial\theta_s}{\partial\tau} = -St_s(\theta_s - \theta_g) \qquad \text{(Solids)}$$

For $\theta^{II}_{sat} > \theta > \theta^{I}_{sat}$

$$(1 + (1 - \tfrac{\theta-\theta^I_{sat}}{\Delta\theta_{sat}})\Psi_{lg})\tfrac{\partial\zeta}{\partial X} = \tfrac{\Psi_{lg}}{\Delta\theta_{sat}}(\tfrac{\partial\theta}{\partial\tau} + \zeta\tfrac{\partial\theta}{\partial X}) \qquad \text{(Continuity)}$$

$$\begin{aligned}&(1 + (1 - \tfrac{\theta-\theta^I_{sat}}{\Delta\theta_{sat}})\Psi_{lg})(\tfrac{\partial\theta}{\partial X} + \tfrac{\partial\theta}{\partial X} + (\theta - \theta^I_{sat})\tfrac{\partial\zeta}{\partial X})\\ &- \tfrac{\Psi_{lg}(\theta-\theta^I_{sat})}{\Delta\theta_{sat}}(\tfrac{\partial\theta}{\partial\tau} + \zeta\tfrac{\partial\theta}{\partial X}) = St_{jump}(\theta - \theta_s)\end{aligned} \qquad \text{(Energy)}$$

For $\theta < \theta^{I}_{sat}$

$$\Psi\zeta = 1 \qquad \text{(Continuity)}$$

$$\frac{\partial\theta_l}{\partial\tau} + \frac{\partial\theta_l}{\partial X} = -St_l(\theta_l - \theta_s) \qquad \text{(Energy)}$$

These equations were then solved using Matlab and the results are discussed in the following section.

3.4 Results and Discussion

Due to higher rate of latent heat of enthalpy injection and high surface heat transfer of packed beds, the temperature of bed reaches the peak saturation temperature as soon as steam front reaches a location in the bed, shown in Figure 3.2. This type of behavior is distinctly different as compared to injection of non-condensible hot gas in the packed bed, where bed never reaches the top temperature of bed[22] due to higher heat loss rate. These results show that this storage process is economically feasible because the bed utilization factor is close to 75% of the bed volume. Higher utilization implies higher energy density and in-turn lower capital costs. During saturated steam injection the condensate hold-up can significantly effect thermal dispersion (discussed in details in the next Chapter) of thermal front.

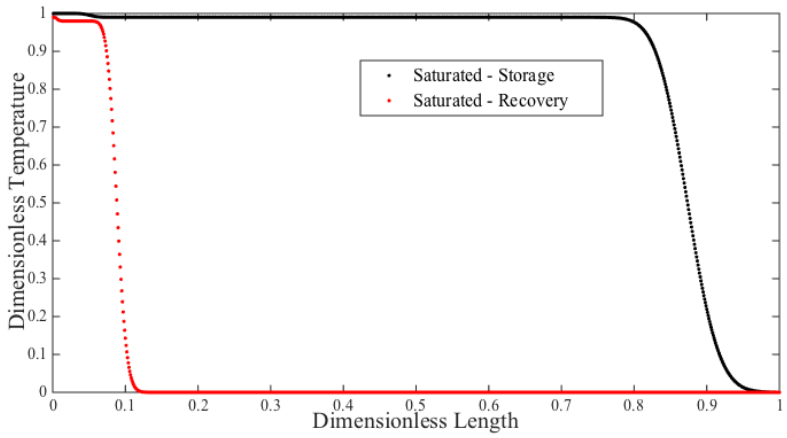

Figure 3.2: *Storage and Recovery cycle calculations for packed bed system with saturated conditions at 50 bars with alumina particles and steam as HTF.*

To demonstrate the model under various conditions, superheated steam is injected in the system. Three totally different processes occur when the superheated steam is injected in the bed. The first is the storage of superheat, similar to the storage of gas. The second process stores the enthalpy of the condensing steam. Third is the storage of heat from the hot water. All three have different time-scales and length requirements. This does not allow for the optimization of all three processes simultaneously as it does in the case of the

much simpler gas HTF. For all three to occur under acceptable conditions, an excessively long storage unit is needed. The length is, in fact, not practical. In the recovery cycle, another problem arises. The main heat storage occurs on the hot particles in which steam has condensed and the water is at the boiling temperature of the saturated steam which is stored. The water cannot be recovered at the same pressure and temperature of the saturated steam whose heat was stored in the particles that are used in the storage unit since the temperature differential required for heat transfer would be insufficient (Figure 3.3). Thus, the pressure in the recovery cycle would need to be lower.

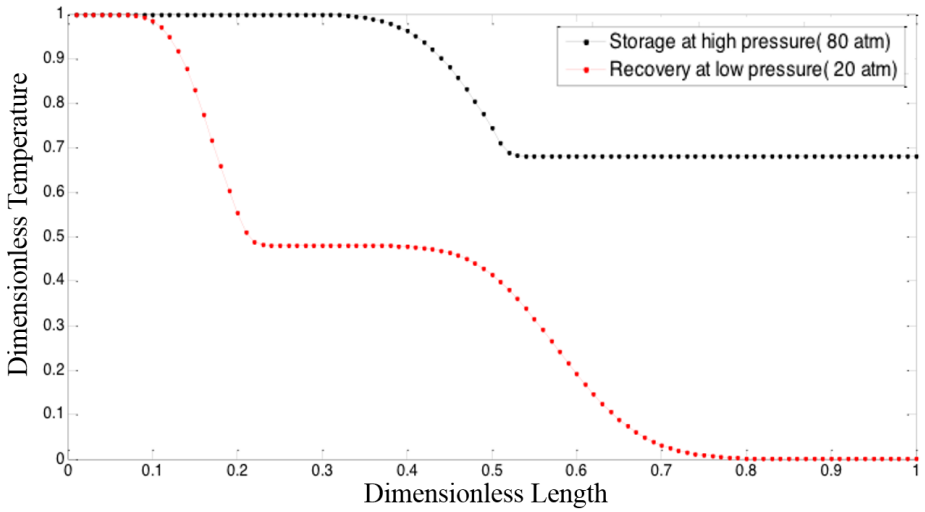

Figure 3.3: *Storage and Recovery cycle calculations for packed bed system with superheated steam injection during storage cycle. Recovered steam is at lower pressure*

This makes superheated stream storage technically and economically impractical. In case of LW-SMRs or other existing LWRs, condition of output steam is saturated which also suits the performance of the packed bed TES systems. However, to accurately model the actual behavior in case of saturated steam the effective thermal dispersion i.e. the effective molecular or eddy thermal diffusion must be modeled. Following chapter discuses the detailed understanding of thermal dispersion in the packed beds upon steam injection.

Chapter 4

Axial thermal dispersion in packed beds

4.1 Introduction

Previous theoretical and experimental studies on thermal performance of randomly packed beds were conducted with air or single phase HTF[22;27]. The previous work included modeling energy storage and recovery cycles, and evaluating the exergy of the system. Similarly there are several other studies[13;14] which have modeled or experimentally studied the behavior of packed bed sensible heat storage systems. Most of these studies model the temperature response of the system in axial or radial direction with time upon injection of hot fluid or cold fluid into the bed during storage or recovery cycle, respectively. Mostly for large scale models axial dispersion inside the bed and heat loss through the walls are sufficient to determine the overall performance of the system. Therefore better understanding of thermal dispersion is essential for the system design of TES. Testu et al. found thermal dispersion coefficients for both air and water flow through a bed of glass beads[33]. They presented the variations of the coefficients with respect to different Reynolds number and Peclet number values. Most of the previous packed bed heat transfer studies found that in practical situations the temperature difference between the solid and fluid phases can be neglected. Thermal dispersion gives

insight on how the type of fluid and flow rate of the fluid influence thermal stratification, volumetric utilization and exergy destruction due to temperature gradients. The type of material and geometry play a vital role in the effectiveness of the heat removal from the fluid. As mentioned before these type of studies have been conducted with HTFs such as air, water, heating oils etc. However, one of the significantly important HTFs – steam, has not been used for these TES evaluation studies.

Steam is one of the most commonly used working fluids for at least 50% of the operating power plants. Most of the solar thermal power plants, which need an efficient and economical TES system for their viability, use steam as the primary HTF and working fluid. Thus storage and recovery of thermal energy from steam can be a critical factor for the future of stable grid and making solar thermal energy a viable option. Apart from TES, there are some other applications as well where steam condensation in packed beds is relevant such as, for enhanced oil recovery steam is injected into the solid inert rocks. The purpose of this is not intended for design or analysis of a particular application system but broader understanding of thermal behavior inside packed bed upon steam injection.

Direct steam condensation in packed beds of solids have been studied and tested with different perspectives such as for separating water vapor from air[34–36]. Although the technical scope of these studies were different from the current study, the complexity of the phase change in the packed bed type complex geometry still plays dominant role. The effect of pressure changes at the interfacial zone and how the equilibrium temperature of the packed bed changes – are some of the questions which have not been addressed fundamentally and require very sophisticated instrumentation or modeling techniques for fundamental understanding. The scope of this study does not include the effects of steam condensation on momentum transport but will be limited to thermal transport. Thermal dispersion in a porous media results from a combined effect of conduction or heat diffusion and convection. A homogeneous porous medium of spherical particles randomly packed in a cylindrical column is the geometric description of system considered here. The importance of this geometry and material used are discussed in later sections. The large surface area provided by the numerous small particles allows for the HTF to transfer its energy to the solid particles in a

radially uniform manner. This ensures a stable condensation flow rate from the packed bed. Upon steam injection, the bed can be divided into three zones - hot vapor zone, mushy or liquid-vapor mixture zone and cold liquid zone. Due to the transient nature of this problem the relative thickness of these zones will change continuously and understanding this quantitatively will require a complex flow instrumentation and detailed models of coupled momentum equations for two phases with variable local pressures. However, as stated earlier the scope of this study is only limited to spatio-temporal thermal behavior only. An inverse formulation of this problem was presented analytically and experimentally by Woods et al.[37]. They studied thermal response of injected cold liquid inside the bed of hot rocks which leads to formation of moving vaporization front and assuming constant velocity of the fluid phases an analytical similarity solution was derived and validated.

Condensing steam flow in a packed bed involves various multi-physics processes such as condensate nucleation, surface capillarity effects, condensate or liquid percolation, time scale of dewetting versus heat diffusion in solids, intense density changes in the bed etc. Some of these phenomenon have been previously studied using computational models or separate effect experiments. Wang et al.[38] studied two-phase liquid vapor momentum and energy transport models in porous media. An experimental and computational study was conducted by Udell[39] where upon application of external heat, phase change and fluid motion for the single component fluid was modeled and experimentally studied. As the steam passes over the particles the heat is transferred through different modes: both advection and conduction from the fluid in both liquid and vapor phase to the solid. The steam injection process in relatively much colder packed bed is associated with continuous phase change which implies there is a large amount of energy injected per unit time and unless the flow rates are very low it will be difficult to observe the distinguishable effects of energy deposition in the packed beds or in other words those beds can get saturated very quickly. The condensate percolation is expected to be very complex and the associated cross-linked thermal conduction due to these condensate channels will be very complex. The effect of steam flow rates on thermal dispersion in the beds is one of the goals of this work. The roles of diffusion and advection at the particle scale or for a homogeneous local volume requires solution of the local thermal

energy transport quantification. The experimental and theoretical models are developed and presented in this chapter to examine the effects of steam flow rate or the energy input rate on the thermal response of bed in equilibrium with fluid medium.

4.2 Experimental Methods

4.2.1 Design Objectives

The design of this experimental set-up originated from previous experiments that utilized a cylindrical vessel for thermal energy storage system constituting randomly packed bed of alumina particles with air as heat transfer fluid[22;40]. These previous results assumed that packed bed configuration enables the uniform flow and temperature distribution in the radial direction i.e. direction normal to the flow. However, due to wall heat losses, the temperature of the wall and the bed were different from each other. So accurate analysis requires simultaneous wall temperature measurements. Alumina particles, i.e. packing media, have high heat capacity, high thermal conductivity and chemical inertness which allow the rapid localized equilibration of thermal energy between fluid phase and solid phase. The material is also non-degradable allowing it to last a long time and remain stable through multiple cycles. Large heat transfer surface area due to considerably smaller particle or packing size as compared to the overall bed dimensions makes the thermal front propagation more predictable and very steep along the flow direction. With saturated steam as the heat transfer fluid, rate of heat injection is much faster during condensation process, thus if the media has sluggish response to absorb heat this will lead to very complex energy balance in three phases. Moreover the results of previous material behavior studies[41] showed no changes in physical characteristics of alumina particles under steam condensation and boiling cycles. Therefore, choice of alumina particles will meet the crucial design objective of performing reproducible thermal behavior tests. As one of the prime objectives is to understand the axial dispersion of temperature front upon steam injection, temperature must be measured at various locations in the axial direction without interfering significantly with the system

behavior. The scope of this study is limited to steam condensation at atmospheric pressure which simplifies the design of the vessel and fittings. One of the difficult part in understanding steam condensation process is associated with the uncertainties in the flow conditions and thickness of the two phase (liquid-vapor) zone inside the packed bed. Moreover, effective thermal conductivity inside the bed is strongly dependent upon instantaneous liquid hold-up and interface location. Therefore condensate flow rate must be measured or estimated throughout the experiment to correlate with the temperature response.

4.2.2 Experimental Setup

The cylindrical quartz tube randomly packed with spherical particles was chosen as the main test chamber for this experimental set-up following the design objectives described before. The size of the tube was 15.24 cm tall and 6.35 cm diameter, and the design limitations on the size were only on the diameter because of the standard ceramic flanges used to seal the ends and size of the particles or packing material. The size of 3 mm is considered as an optimum size for thermal packed beds as examined in the previous studies based on balance between thermal performance and pressure drop requirements[22] . The ratio of the tube diameter to particle diameter greater than 20 allows for the plug-flow assumption or radially uniform dispersion of the thermal front. The thermal storage test media was chosen to be spherical alumina particles procured from Norpro with the commercial name Denstone-99 particles. These commercially available spherical particles were considered for this experiment as they allowed uniform isotropic heating, and have been tested for their chemical inertness and robust thermo-mechanical behavior[41] with steam. The vessel to house alumina particles was made of quartz tube sealed with ceramic flanges at both ends to avoid energy losses from the boundaries. The visual inspection of motion of liquid-vapor interface can be done with the quartz tube and known constant emissivity value of quartz material in temperature range $(25°C - 100°C)$ which allows easy measurement of wall temperatures with IR camera.

The measurement set-up to attain the temperature values along the outside wall of the heat sink vessel was a FLIR infra-red camera. The packed bed temperatures were measured

with a multi-point thermocouple tube, customized product obtained from Omega Inc. to record the temperature at six axial locations in the bed. The multi-point thermocouple was positioned as close to the center of the bed as possible using a fitting screwed into the top flange of the vessel. Each thermocouple was numbered respective to its position from the inlet of the test chamber.

In-house steam supply was used to conduct these experiments and before starting the experiments it was ensured that steam supply pressure and flow do not change for the duration of the individual experiments. This was done by allowing the steam to condense in a cylindrical flask with cold water and change in the level was monitored with time during steam flow. In addition, during the actual experiments of steam injection in the packed bed condensate flow was monitored to take into account the uncertainities. It was found that the flow rate of steam at set valve conditions remained within 5% of the measured mean value. Steam was supplied from the top of the test chamber after passing through a pressure regulator holding the back pressure constant for all experiments. A globe valve was situated just before the entrance to the test vessel to allow control of steam after the supply valve was opened to allow steam to pass through the regulator. This combination allowed the evaluation of system's response to a step input of constant pressure steam. The downstream end of the test chamber was connected to a tube-in-tube heat exchanger where the remaining vapor was condensed. This extra step allowed the accounting of the total mass flow rate of steam that passed through the chamber to be collected and measured, enabling a value for the total amount of energy input into the system to be obtained. A simplified schematic of the experimental setup is shown below in Figure 4.1.

In addition to experiments with steam, the set-up was designed to allow the experiments with other HTFs as well. A teflon heater strip was retrofitted to a two foot section of piping allowing for air to be heated prior to entering the packed bed. The thermal response of the bed with hot-air and steam was one of the important analytical experiments to understand the comparative difference between two different fluids. Another purpose of air injection system was to provide cold dry conditions in the bed after each experiment. This approach ensured consistent initial temperature for each of the experiments and improved repeatability

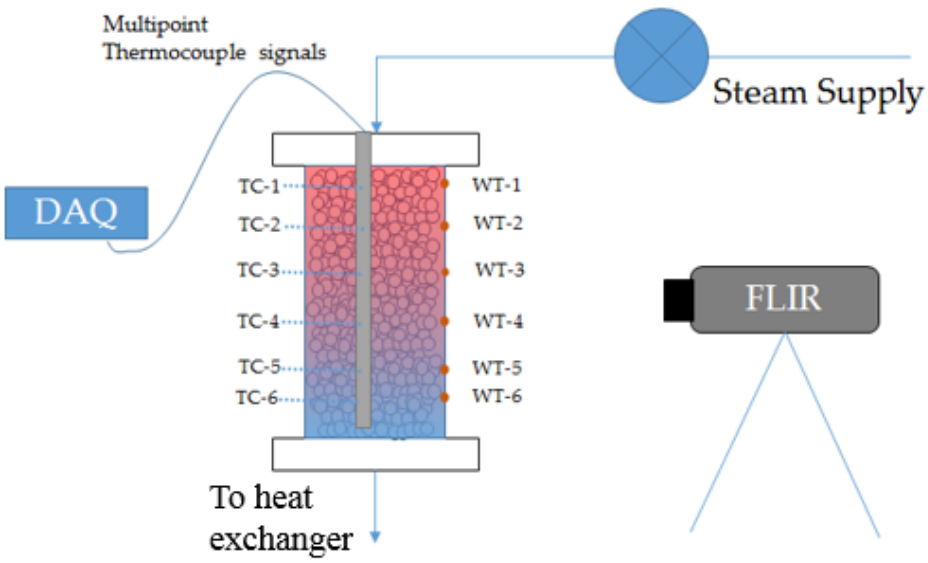

Figure 4.1: *Schematic of experimental steam setup of packed bed heat sink consisting of a clear fused quartz tube, alumina particles, multi-point thermocouple, steel piping, steam supply, and FLIR camera.*

between experiments resulting in reliable data.

Experimental Procedure

The steam injection experiments were performed in two sets. The first set of experiments were slow injection experiments where already regulated steam supply at atmospheric pressure was further throttled by a globe valve to nearly lowest flow rate. The pressure regulation to atmospheric pressure was confirmed with the experimental data of steam temperature of $100°C$. Steam was then continuously injected through the bed until the images continuously recorded by thermographic camera showed that the wall of the cylinder had achieved steady state conditions.

In the case of the fast injection tests, the globe valve opening was increased to nearly double the flow rate. Same procedure was repeated as described for slow injection case. The injection flow rate of the steam for each case was determined by measuring the condensate collected per unit time. Multiple experiments were performed to ensure repeatability and consistent flow rate values for both the slow and fast measurements. Compressed air was used after the steam supply was shutoff to remove trapped condensation in the packed bed

for complete measurements.

Air as a single phase HTF was heated and sent through the randomly packed bed. The flow rate of the air was controlled with an air compressor and its outlet nozzle. The air was allowed to reach a steady state temperature by bleeding out through a valve located just before the packed bed and once it had reached the steady temperature the inlet and bleed valves were slowly opened and closed, respectively. This allowed the pressure to relatively not change so that the air at consistent temperature would enter the packed bed without any uncertainties.

4.3 Model Definition

The modeling of heat and mass transfer in packed beds has been studied extensively in the past. Various phenomenological models based on previously conducted experiments exist in the literature for parametric heat transfer evaluation. It has been shown previously by many that packed bed systems with high tube to particle diameter ratio (>10) can be treated as plug flow for wide range of Reynolds numbers. There are generally two approaches to model heat transfer between solids and fluid in a packed bed arrangement. One approach of modeling this phenomena is by assuming homogeneous media with an assumption that both solid and fluid are in local thermal equilibrium at all times. Another approach is to model the system with two equations, for solid and liquid phases, coupled to each other via solid to liquid interfacial heat transport term. It was shown earlier that for small particle size and high thermal conductivity, the two phases can be considered in equilibrium with each other[22]. Therefore, one-equation model is sufficient for the system considered in this study as the conditions for fluid-solid thermal equilibrium are satisfied. In this chapter, we briefly describe our modeling approach based on one dimensional convection diffusion model.

$$(\epsilon\rho c_{pf} + (1-\epsilon)\rho c_{ps})\frac{\partial T}{\partial t} + \epsilon\rho c_{pf} v\frac{\partial T}{\partial x} = k\frac{\partial^2 T}{\partial x^2} - \beta_w(T - T_o) \tag{4.1}$$

The boundary condition at the inlet plane is defined as

$$T(x=0) = T_m \tag{4.2}$$

where, T_m is the steam inlet or saturation temperature at atmospheric pressure, and no axial heat transfer near the outlet leads to boundary condition,

$$\frac{dT}{dx}(x=H) = 0, \tag{4.3}$$

and initial condition

$$T(x, t=0) = T_o. \tag{4.4}$$

In order to non-dimensionalize the differential equation and boundary conditions some of the the quantities can be defined as, the ratio of thermal capacity of the fluid phase to the thermal capacity of mixture

$$\kappa = \frac{\epsilon\rho c_{pf}}{\epsilon\rho c_{pf} + (1-\epsilon)\rho c_{ps}}, \tag{4.5}$$

thermal diffusivity,

$$\alpha = \frac{k}{\epsilon\rho c_{pf} + (1-\epsilon)\rho c_{ps}}, \tag{4.6}$$

and non-dimensional wall heat loss coefficient

$$\beta = \frac{\beta_w}{\epsilon\rho c_{pf} + (1-\epsilon)\rho c_{ps}} \tag{4.7}$$

Substituting these quantities in Eqn. (4.1) and using the non-dimensionalization on space, time and temperature defined in the nomenclature leads to a non-dimensional equation (4.8)

$$\frac{\partial\theta}{\partial\tau} + \kappa\frac{\partial\theta}{\partial X} = \frac{1}{Pe}\frac{\partial^2\theta}{\partial X^2} - \beta(\theta - \theta_o) \tag{4.8}$$

with non-dimensional boundary conditions

$$\theta(X=0)=1, \tag{4.9}$$

$$\frac{d\theta}{dX}(X=\frac{H}{D})=0, \tag{4.10}$$

and initial condition

$$\theta(X,\tau=0)=\theta_o. \tag{4.11}$$

Substituting $\phi=\frac{\theta-\theta_o}{1-\theta_o}e^{-\beta\tau}$ simplifies the differential equation with boundary and initial conditions to

$$\frac{\partial\phi}{\partial\tau}+\kappa\frac{\partial\phi}{\partial X}=\frac{1}{Pe}\frac{\partial^2\phi}{\partial X^2} \tag{4.12}$$

$$\phi(X=0)=e^{\beta\tau} \tag{4.13}$$

$$\frac{d\phi}{dX}(X=\frac{H}{D})=0 \tag{4.14}$$

$$\phi(X,\tau=0)=0 \tag{4.15}$$

The term $\frac{L}{D}>>1$ as the physical dimension of test bed is much larger as compared to the diameter of the particle. As a result, this problem can be considered as a semi-infinite region problem. The solution to this semi-infinite region problem has been derived previously in the literature[42] and this algebraic form of solution will be used for the predictive thermal model.

$$\phi(X,\tau) = \frac{1}{2}\exp(\beta\tau)[\exp(\frac{(\kappa-\lambda)Pe}{2})erfc(\frac{X-\lambda\tau}{2}\sqrt{\frac{Pe}{\tau}}) + \exp(\frac{(\kappa+\lambda)Pe}{2})erfc(\frac{X+\lambda\tau}{2}\sqrt{\frac{Pe}{\tau}})] \tag{4.16}$$

where, $\lambda = (\kappa^2 + \frac{4\beta}{Pe})^{\frac{1}{2}}$.

Both advection and diffusion components of thermal energy transport play some role in the energy exchange process between fluid and solid. However, due to transient liquid hold-up amount in the packed bed along the motion of the steam front, the diffusion component will vary in time and position as thermal conductivity of water-liquid is approximately 10 times than that of steam at that pressure. Due to difficulty in modeling steam condensation behavior and two phase behavior in this complex geometry, this simplified model is adopted to this various thermal diffusion component based on the approach of steam front to a particular location in the bed. This work models the problem in vapor or liquid phases and as the steam front approaches a particular location, the diffusion component is modified corresponding to steam properties instead of water properties.

The next section will discuss the experimental results and comparison of the experimental data to the analytical solution.

4.4 Results and Discussion

4.4.1 Experimental Results

The experimental results are discussed first, followed by a comparison of the analytical solutions to the experimental data. The justification for these steam condensation experiments was described in the introduction along with the requirements for uniformity of radial flow and condensation process in the packed bed. The thermal images along the wall of the packed bed as obtained from the IR camera for one of the experiments are shown in Figure 4.2. These images show that there is no angular non-uniformity in the bed. Although

temperature of walls is lower than the temperature of the bed, shown later, as obtained by internal thermocouples. Moreover, X-ray images shown in Figure 4.3 also indicate radially uniform condensing front. These results show that 1-D axial model with wall heat losses is sufficient for thermal behavior prediction.

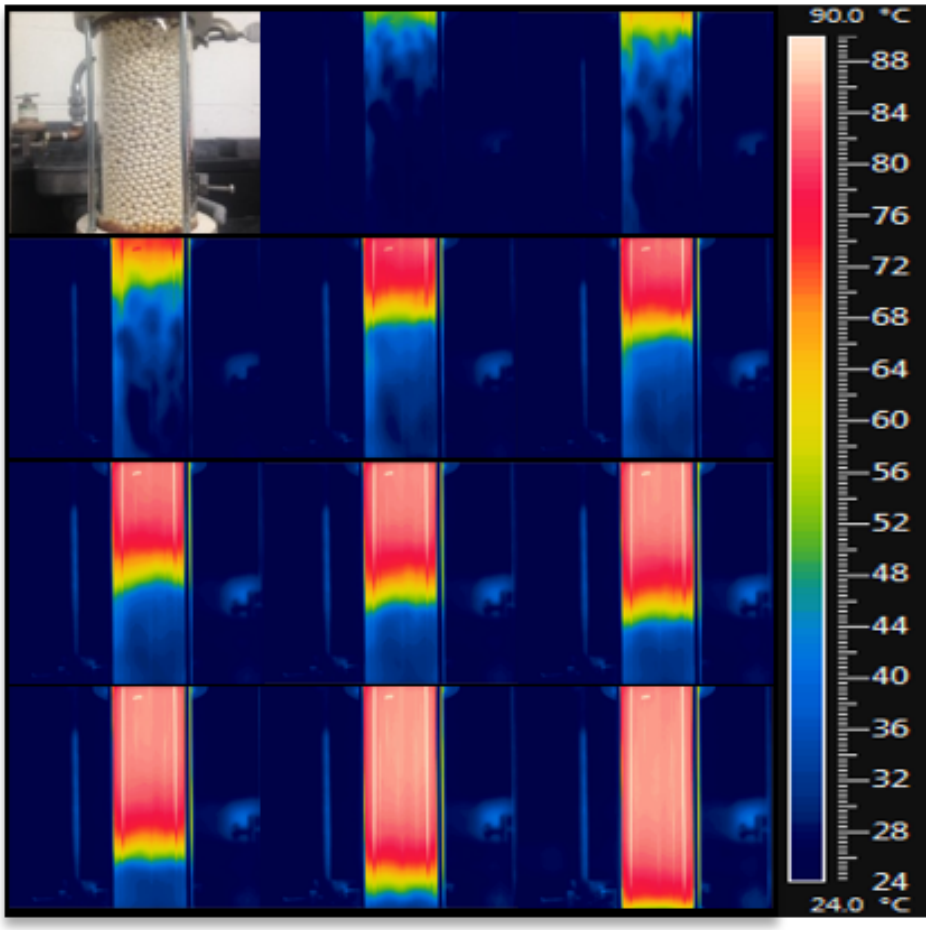

Figure 4.2: *(TOP LEFT) Picture of experimental packed bed vessel. (LINE WISE: LEFT to RIGHT) Time step images from FLIR software for an experimental run at 50 psi for; 5, 10, 15, 20, 30, 35, 40, 45, 50, 60, 70 seconds after steam injection, respectively.*

The propagation of the temperature front for each of the different cases, injection rate and HTF type, while penetrating the randomly packed bed was experimentally studied. The differences between the different steam injection rates will be discussed next. The average condensate collection flow rates for the slow and fast cases were measured to be, respectively, 6 cm^3/s and 12 cm^3/s. The discussion provided in the next subsections will not explicitly mention the flow rates but will use terminology of fast and slow injection.

For each experiment it was found that the uncertainty in the measurement of condensation collection flow rate is within 5% of the numbers sated above.

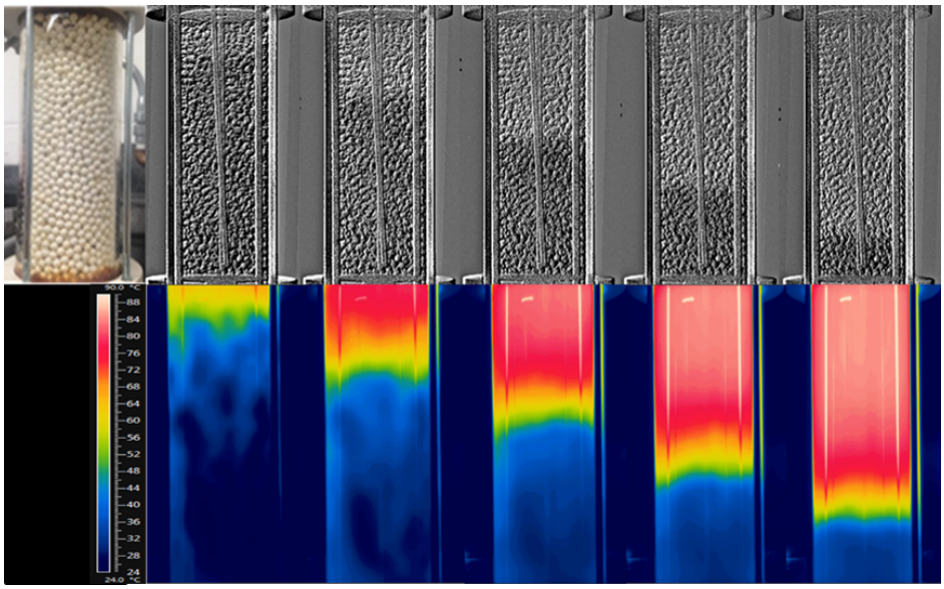

Figure 4.3: *(Top Left) Image of 6" packed bed with Alumina particles. (Top) X-ray images of packed bed and (Bottom) IR images in 10 second intervals during slow steam injection.*

Slow steam injection

The characteristic thermal response of the packed bed system at different times upon slow injection of steam is highlighted in this discussion with explanation of results. Upon injection of steam into the bed, there are two thermal transport mechanisms- advection and conduction modes at different spatial locations and different time frames. Near the entry port where steam is introduced, in this present experimental set-up from the top, in a very short time interval temperature of the bed and fluid streams become almost equal to the steam inlet temperature or saturation temperature. With the steam supply continuously available, irrespective of injection rate, the bed temperature at the top is always maintained at a constant top temperature i.e. saturation steam temperature. This constant bed temperature at the top will conduct heat from the top to bottom of the bed due to non-negligible thermal conductivity of alumina particles and water condensate in the bed i.e. conduction mechanism. Simultaneously, due to steam injection in the bed it is carrying some amount

of energy as it moves in the bed i.e. advection mechanism.

Due to slow injection rate, initial rise in the temperature at axially farther locations will be dominated by the conduction mechanism. As the steam or two phase mixture front, which is at temperature near the saturation temperature, reaches those regions located far away from injection point there is a sudden change in the temperature. This effect can be seen from temperature measurements obtained by thermocouples at different locations and at different times as shown in Figure 4.4. The rate of increase of temperature for different thermocouples positioned at different axial locations is divided into two distinct regimes with two distinct slopes, especially for last four (3-6) locations. The initial regimes, which show lower slope are governed by conduction mechanism and later regimes with higher slope, are governed by advection. These conclusions are substantiated with the observations that conduction effect shows an observable conduction dominate temperature plot for locations at larger distances from injection point. Similar effects were quantitatively predicted and experimentally observed by Woods et al. in liquid-vapor flows around porous beds[37;43]. In theses previous studies by Woods et al., cold water was injected into hot rocks.

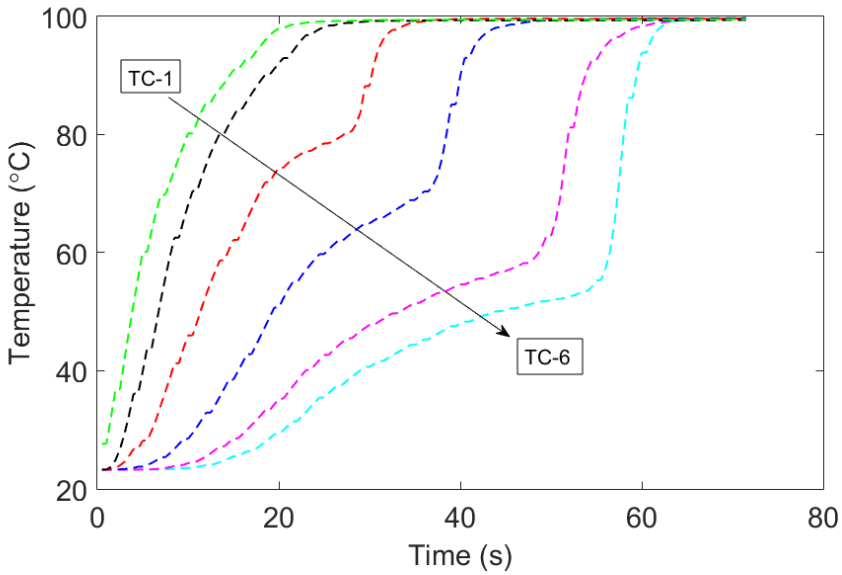

Figure 4.4: *Slow injection steam case experiment results*

Fast steam injection

Based on the explanations provided in previous subsection, it is expected that advection term will be higher in fast injection experiments as compared to the slow injection experiments. The higher advection term implies that total amount of influx enthalpy carried by the steam or two-phase mixture is much higher and thus, as the fluid stream moves through the bed it is equilibrating the bed to the saturation temperature at almost constant rate at all spatial locations. Due to much higher rate of enthalpy injection in the bed due to advection term, the effects of conduction will not have much impact on the rate of temperature increase in the bed. The results in Figure 4.5, for fast injection, confirm this explanation. This phenomenon of smaller temperature dispersion due to conduction can be seen in the experimental results of fast injection experiments.

Compared to the slow injection case, the time taken for the bed to reach peak temperature throughout in the fast injection case is smaller.

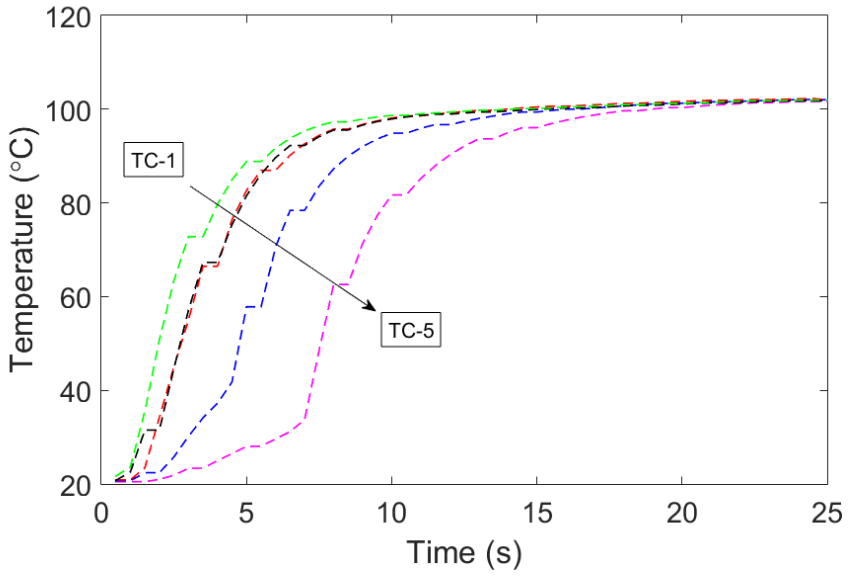

Figure 4.5: *Fast injection steam case experiment results*

4.4.2 Air injection

One set of results with the air as HTF are displayed in Figure 4.6, as the difference in flow rate caused no significant difference in the thermal front propagation in the packed bed. The top temperature at each axial position is at lower temperature going from the inlet to exit of the vessel. This results in a more elongated thermal front as compared to the case with slow steam injection. Another characteristic to be noticed is that unlike steam, the air experiments do not show the abrupt change in slope.

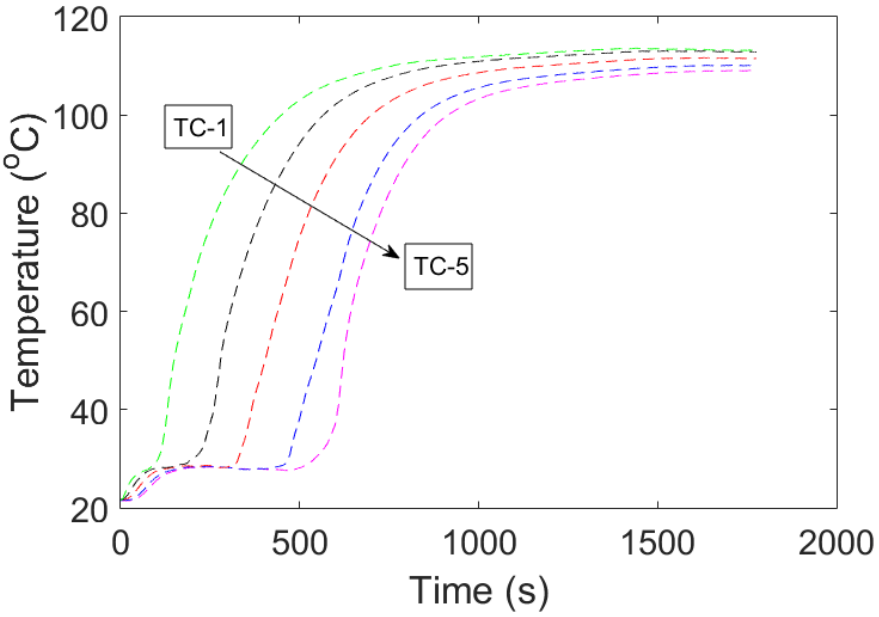

Figure 4.6: *Air injection case experiment results*

The comparison of experimental data with air and steam as HTFs shows there are some very distinct observations which can be made. Due to the low energy density of air it takes a longer time to heat the packed bed and even in the steady state situation the rate of heat loss through the bed walls are comparable to the rate of heat input injected in the bed. This leads to temperature gradients within the bed even after a continuous steady state, as can be seen in Figure 4.6 where the time series plots of different thermocouples show that lower end thermocouples remain at lower temperatures with steady state condition. Whereas the high energy density of steam because of the latent heat allows it to saturate the packed bed to top temperature more quickly and it can be seen in Figures 4.4 and 4.5.

4.4.3 Analytical results and validation

The analytical model as described by Eqn. 20 is used to predict thermal behavior inside the bed. For the slow injection case with assumption of constant velocity throughout the packed bed for the steam condensation front, the plot for the analytical solution along with experimental results are shown in Figure 4.7. The model parameters used for the analytical solution are listed in the Table 4.1.

Coefficient	Slow	Fast
$(\frac{1}{Pe})_W$	0.0094	0.0046
$(\frac{1}{Pe})_S$	0.0006	0.0003
β_W	-0.1	-0.1
β_S	-0.0001	-0.0001
κ_W	0.12	0.03
κ_S	0.06	0.03

Table 4.1: *Diffusion and advection coefficient values for the analytical solutions for steam injection.*

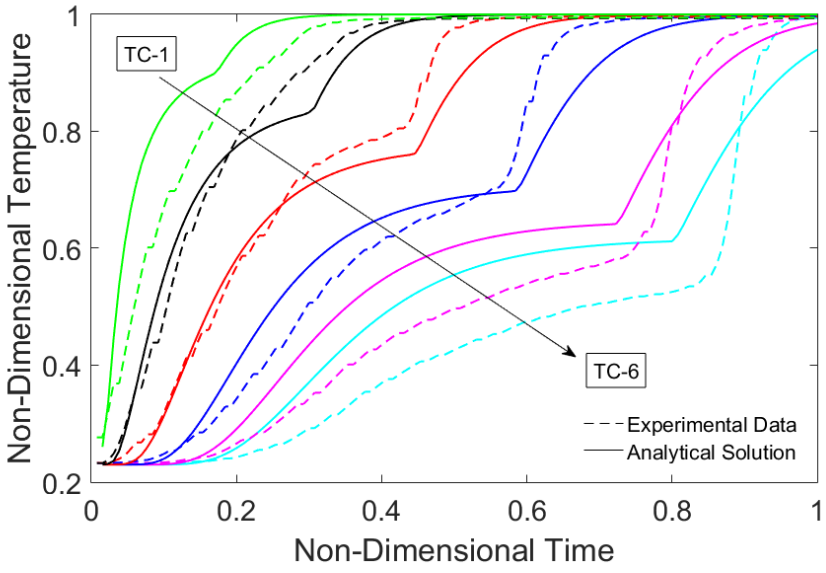

Figure 4.7: *Slow injection steam case compared to analytical solution with constant velocity.*

From the plots it can be inferred that the analytical and experimental solutions show similar trend for most of the thermocouples and for all times. Some discrepancies especially

at the farther thermocouples may be because of constant velocity assumption. With data from different experiments, it was observed that the condensate flow rate decreases as steam front progresses in the bed. Using measured flow rates from different experiments, flow rate vs bed length data was obtained and plotted. The flow rate results for each case were averaged and the plot in Figure 4.8 shows the trend-line that was found for the data.

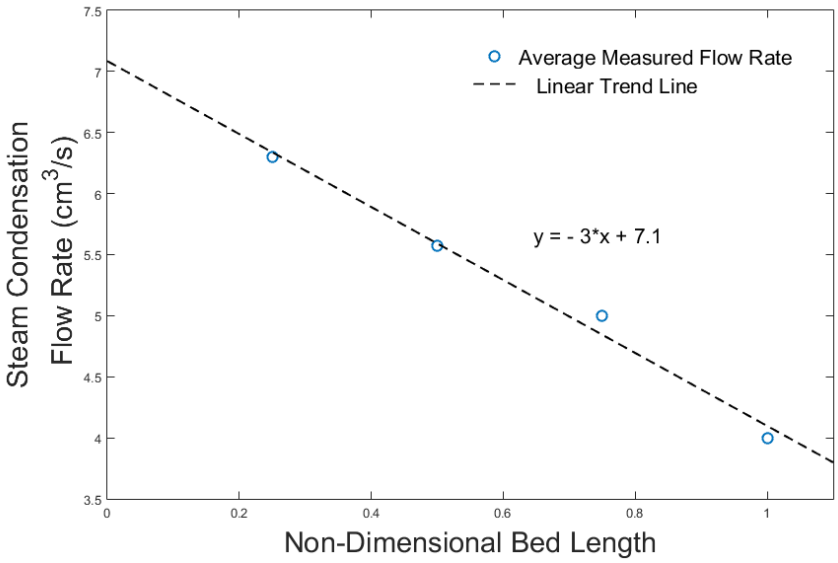

Figure 4.8: *Slow injection steam case, steam condensation flow rate trend-line for a varying steam condensation velocity at different depths within the packed bed during*

This linearly changing velocity was then used in the analytical solution to acquire the new solution which is shown in Figure 4.9. From these plots, it is clearly evident that the use of a varying velocity results in closer predictions to the experimental data.

Similarly, for the fast steam injection case the solution was solved with a constant and varying velocity, which are shown in Figures 4.10 and 4.11, respectively. Comparisons show that the model performs much better for slow injection case as compared to fast injection case. This can be attributed to the higher degree of uncertainties in the flow measurements in the fast case.

The validated analytical model for both slow and fast injection cases can be used for different case studies and design investigations. One of the important critical parameters as highlighted before is axial dispersion. Although the model developed and experimental

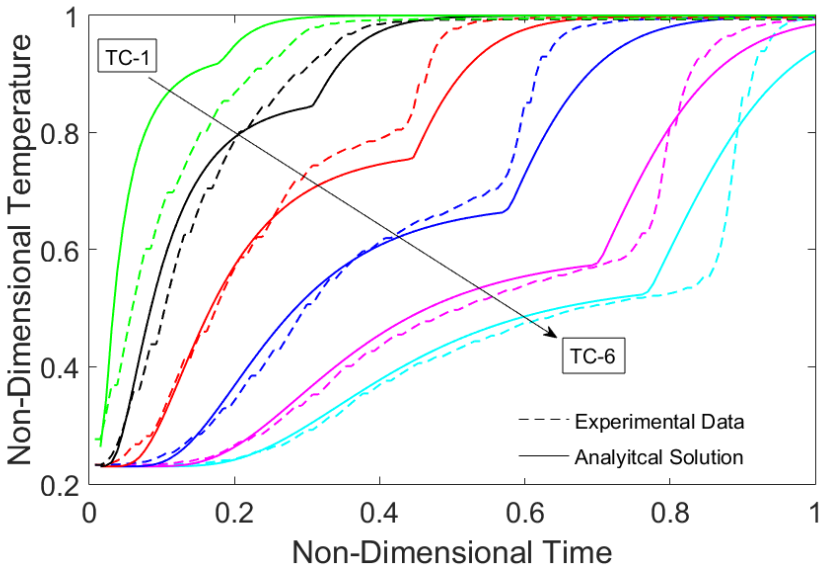

Figure 4.9: *Slow injection steam case compared to analytical solution with varying velocity*

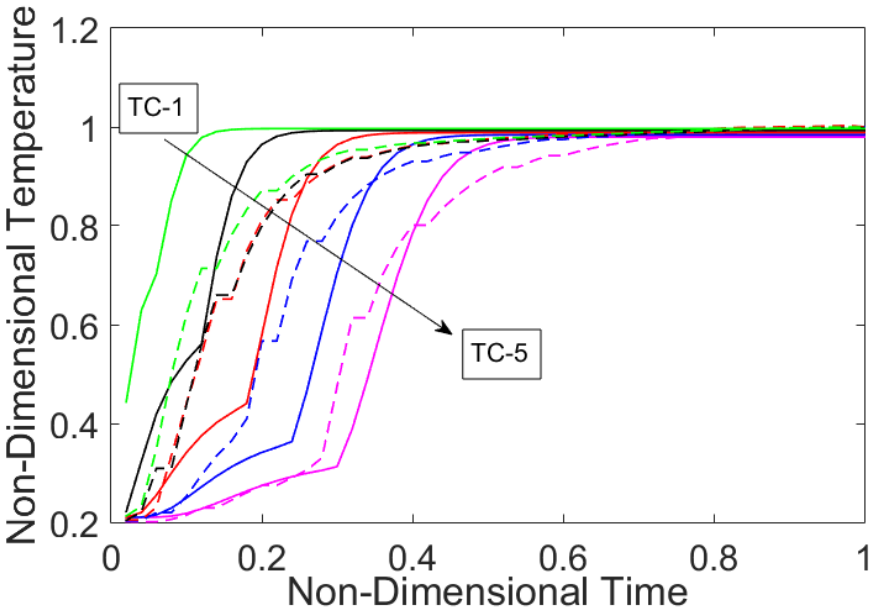

Figure 4.10: *Fast injection steam case compared to analytical solution with constant velocity.*

studies conducted highlight the effect of axial dispersion on the time series curves shown in Figure 4.12, the explicit relationship between temperature vs axial dimension can help in developing better understanding of the effects of steam injection. The temperature vs axial dimension plots for different times are shown in Figures 4.12 and 4.13. It can be

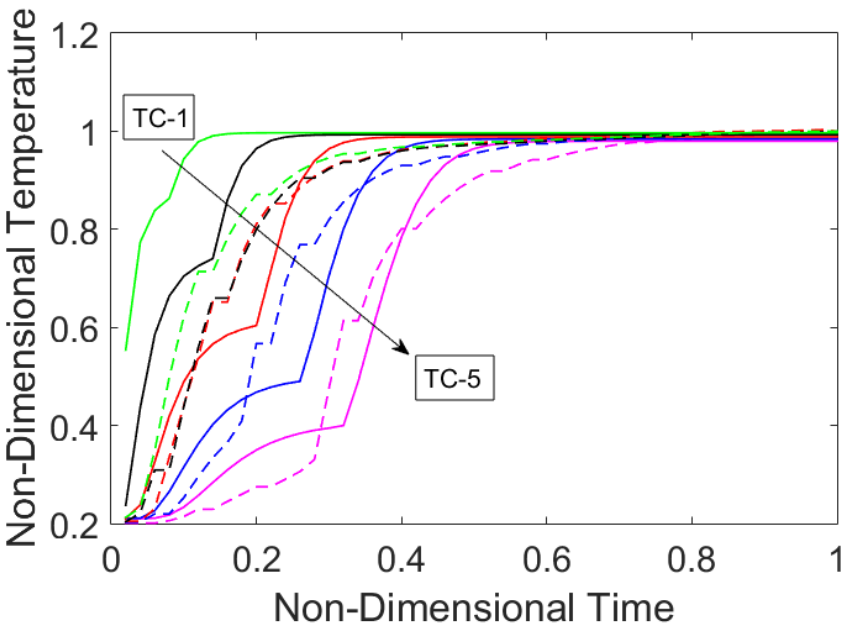

Figure 4.11: *Fast injection steam case compared to analytical solution with varying velocity.*

inferred the slow injection case due to dominate conduction effects experience less steeper temperature dispersion as compared to the fast injection case for different times. Even though 1-D model is validated it is difficult to ascertain the scalability due to complex nature of the process. Therefore, high fidelity temperature measurement technique was deployed to further understand thermal dispersion.

4.5 Higher Axial-Spatial Resolution Experiments

4.5.1 ODiSI-B

Higher temperature resolution can be obtained with a Rayleigh backscattering based distributed optical temperature sensor (DTS). A DTS system developed by Luna Inc., called ODiSI-B, was installed in the packed bed using a custom made probe sheathed in stainless steel to protect from crushing the fiber. The Luna ODiSI B senses temperatures and stress levels using fiber optics in conjunction with a tunable laser source, as shown in Figure 4.14. The technology consists of distributed optical fibers that utilize Rayleigh scattering to sense

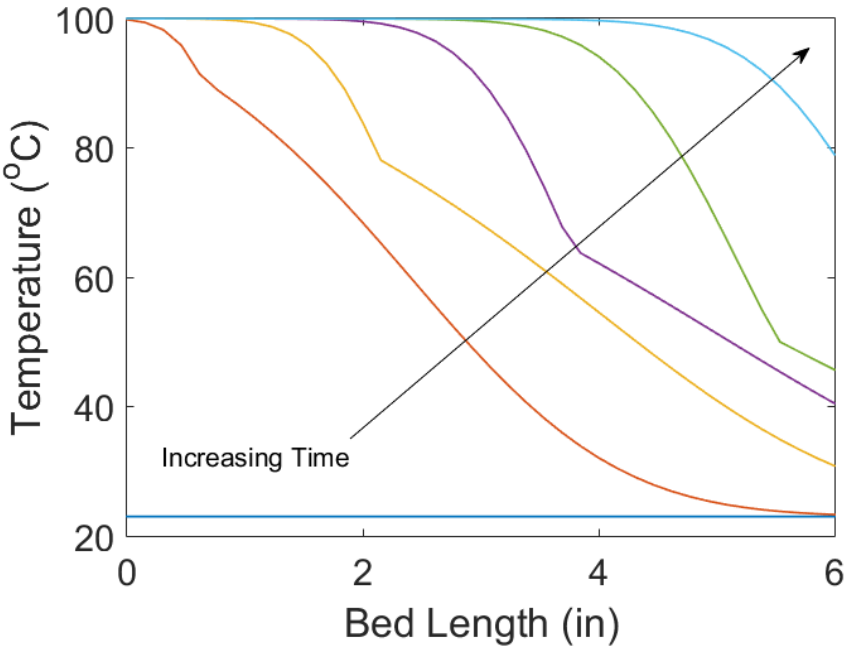

Figure 4.12: *Temperature plotted against bed length for slow injection analytical solution with varying velocity. The time step is 3.6 seconds from 0 to 18 seconds.*

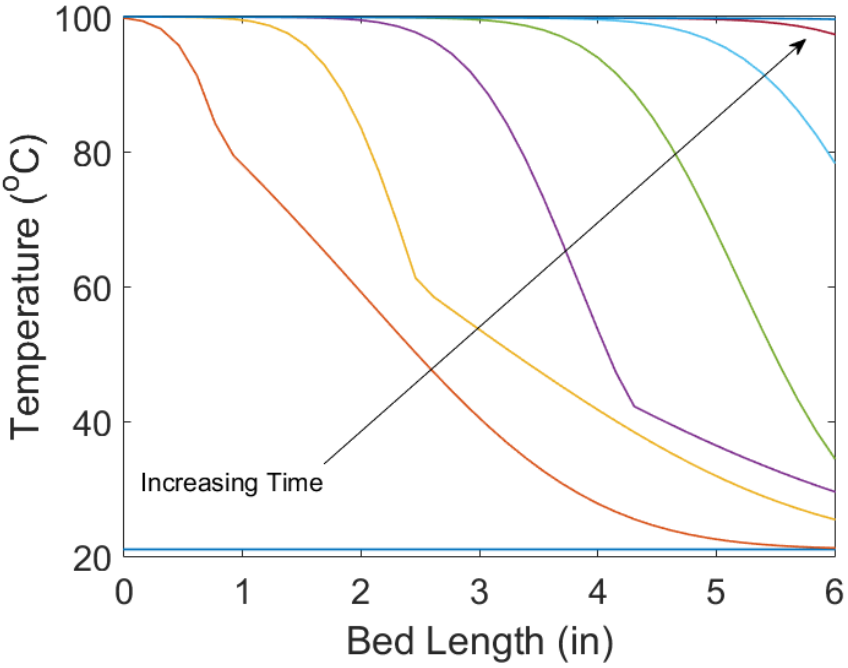

Figure 4.13: *Temperature plotted against bed length for fast injection analytical solution with varying velocity. The time step is 1.8 seconds from 0 to 12.6 seconds.*

small defects in each fiber's construction. The defects cause a difference in the index of refraction, shown in Figure 4.15, creating Rayleigh backscattering at the location of these defects. These backscattering profiles are produced using a Mach-Zehnder interferometer. Sensors are aligned along the fibers in an array pattern. Using interference frequencies found from coherent optical frequency domain reflectometry (c-OFDR) technique, the changes in sensor length are then proportional to the frequency created. Sensors are identified based on a keyed profile and when a match is found, the stored spectrum is used as a base spectrum for all other values to measure in the spectrum. Temperature and strain measurements made using optical sensors can reach spatial resolution increments of 2.5 millimeters. Using fused silica fibers, SiO_2, with diameters of 150 microns, strain or temperature measurements can be made along the fibers using laser technology and known embedded imperfections in the silica. Embedded imperfections in the fiber cause total internal reflections that can the be detected and recorded. The detector measures the fibers' scan pattern under normal conditions and compares it to the scans during testing conditions to calculate the temperature or strain in each segment.

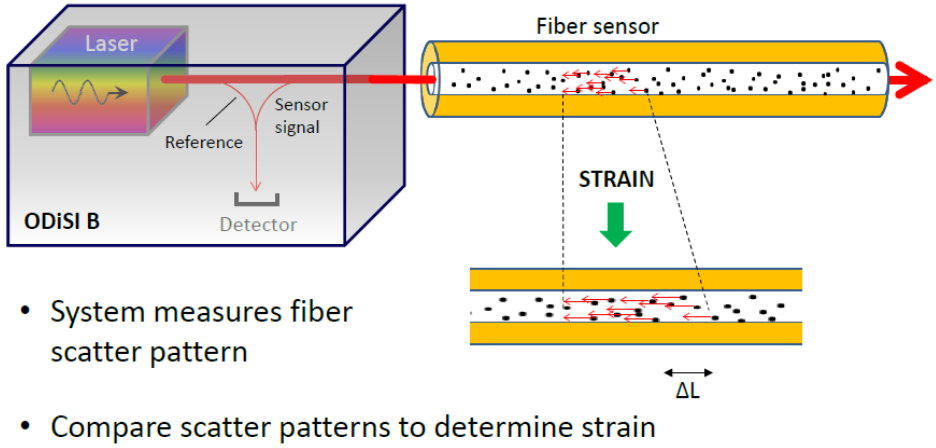

Figure 4.14: *ODiSI-B system showing impurities in fibers that allows laser to read each section of optical fiber.*

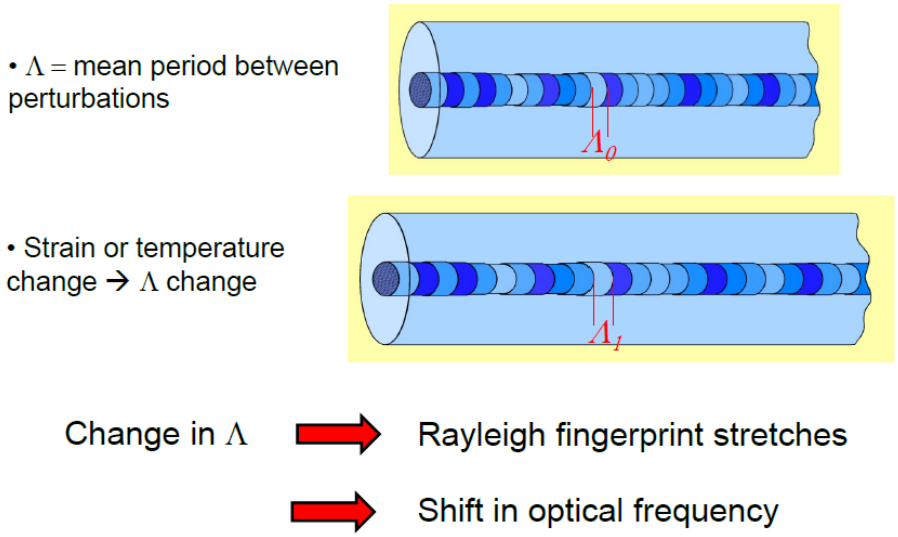

Figure 4.15: *Silica fibers showing individual sections that are measured for shifts in optical frequencies to determine temperature or strain.*

4.5.2 Repeated experiments with ODiSI-B

A foot long quartz tube (diameter of the tube similar to the previous setup) was filled with alumina particles as described before. The ODiSI-B system was installed in this test bed passing through the center of the bed. Figure 4.16 shows the higher spatial resolution for the thermal response of the packed bed during steam injection at rate of 4.5 lb/hr. These measurements show steep temperature gradients or negligible thermal dispersion, i.e. ideal for high efficiency storage. Based on these results a pilot scale model was built for demonstration purposes.

4.5.3 A pilot scale experimental test facility

To demonstrate thermal storage performance on a pilot scale, a new stainless steel vessel was designed and installed with a height of 3 feet (36 inches) and diameter of 14 inches. The packed bed was filled with large rocks (0.5 to 1.5 inch diameters) and tested with saturated steam injection. The testing facility, as detailed in Figure 4.17, incorporated the same in-house steam supply as in earlier tests with now a steam flow meter to measure the flow rate of the steam. The ODiSI-B system was installed with the custom built probe. The

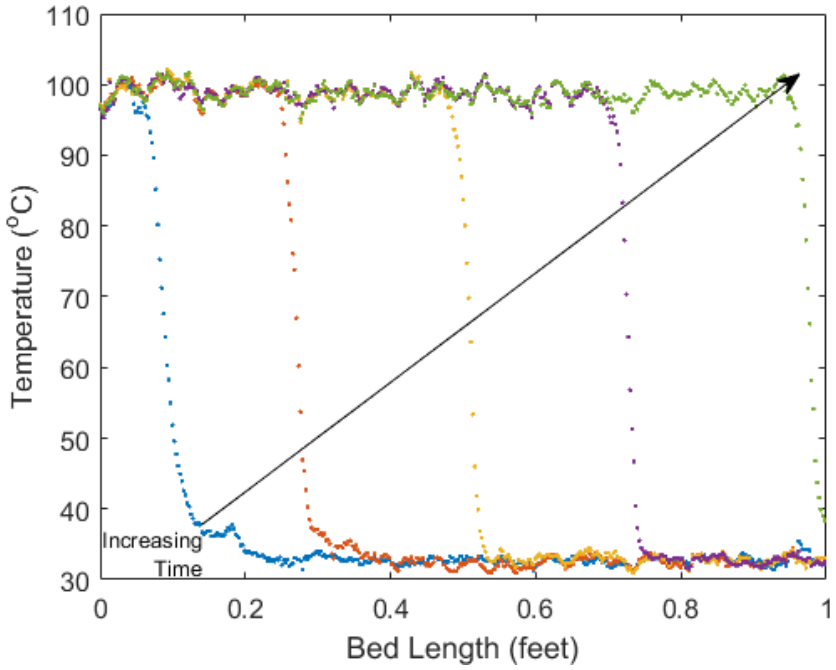

Figure 4.16: *Foot long packed bed thermal energy storage experimental data with optical probe temperature sensor for steam flow rate of 4.5 lb/hr. (20 second time steps)*

multi-point thermocouple used in previous experiments was installed in the side of the new vessel and extended three and half inches into the side of the bed to measure the packed beds temperature radial uniformity near the wall.

Experimental Data

Steam was introduced into the bed at a flow rate of 12.5 lb/hr and the experiment ran for 25 minutes. The thermal response was measured with the temperature sensors and the experimental results obtained from the optical sensor are shown in Figure 4.18. Pilot scale demonstration tests also show steep temperature gradients and low thermal dispersion which makes this method ideally suitable for storing thermal energy of steam.

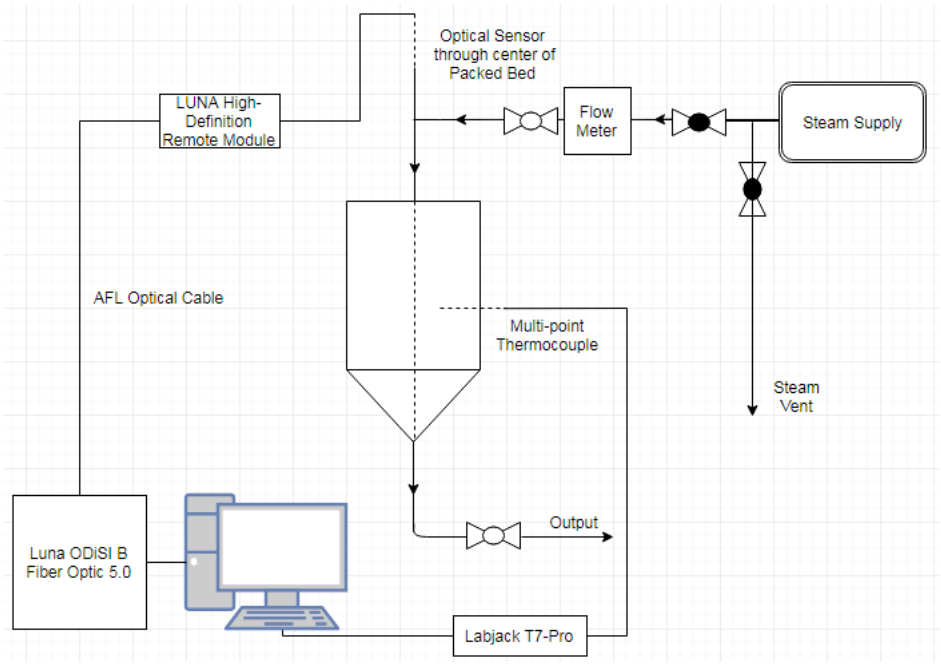

Figure 4.17: *Large packed bed thermal energy storage facility for testing steam injection with optical probe temperature sensor.*

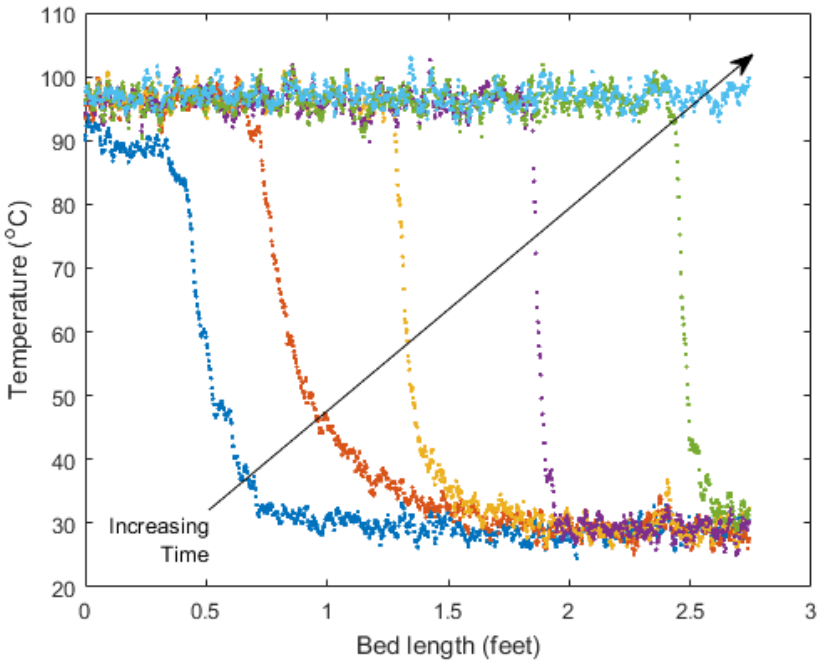

Figure 4.18: *Large packed bed thermal energy storage experiment data showing thermal dispersion in packed bed at different times during 25 minute, 12.5 lb/hr steam injection experiment.*

4.6 Summary

The basic understanding of thermal behavior upon steam injection inside a randomly packed bed of alumina particles was investigated experimentally. The observations show that steam injection at different flow rates result in distinct temperature dispersion curves as compared to single phase heat transfer fluids such as air. The axial dispersion of thermal front is governed by both conduction and advection effects. The conduction effects became apparent for thermocouples located away from the injection points as the steam front or the advection current take longer time to reach those locations. Thus, the slope changes in the temperature dispersion curves become more apparent. The analytical models for the temperature distribution using constant velocity approximation are able to show similar trends as exhibited by the experimental data. The condensate collection measurements show that flow rate reduces as the temperature front progresses through the bed. The performance of the analytical models is substantially improved due to introduction of variable velocity function based on actual measured changes in the condensate collection rate. The flow rate in steam injection experiments played an important role in thermal front dispersion characteristics. Slow injection experiments showed more prominent conduction based thermal fronts as compared to fast injection. Due to these differences in temperature front profiles it can be concluded that in case of slow injection, the temperature at outlet of the bed is at much higher temperature as compared to fast injection case for the same fractional length of the bed at the top temperature. Axial dispersion characteristics are directly observed by conducting experiments in larger scale test beds with high fidelity instrumentation. Fiber-optic distributed temperature sensing system based on the Rayleigh backscattering principle was used to obtain instantaneous temperature profiles. Detailed experiments show that thermal dispersion is negligible in packed beds during storage process.

Chapter 5

Novel packed bed passive safety design for Boiling water reactors

5.1 Passive heat removal system

Recently designed and licensed nuclear power reactors possess significantly more advanced active engineered safety features to reduce the probability of such severe accidents, but the ultimate solution to allay the doubts about nuclear energy rests in passively, or inherently, safe reactors. Inherently safe small modular reactors were envisioned many years ago[44]. These initial passively safe designs were based on both sustaining a long-term subcritical state of the core in all circumstances, and long-term heat removal without any forced circulation requirements. Some of the new reactor designs, and retrofitted existing reactors, have added some passive cooling features, but the knowledge of their behavior envelope in case of unexpected natural events is inadequate. The fundamental basis for passive cooling design is that upon loss of forced circulation, fuel temperature should remain substantially below the melting temperature. As upon safe shutdown, the decay of fission products is the only mode of heat injection into the core, any passively cooled design should be capable of removing this decay heat. There are three possible passive heat transfer modes for the decay heat removal: conduction, radiation, and natural convection. One or more of these

modes are required to reject heat from either the core, reactor vessel, or reactor systems and transfer it into the external surroundings. This process of heat rejection in most of the designs is a two-step process. In the first step, the decay heat is transported from the core internals either to the surface of the reactor vessel or to some other system that can directly interact with environment. Next, heat is transferred from the reactor vessel surface, or similar component, to the atmosphere via radiation or natural convection. This latter step is largely dependent upon civil construction, effective exposed surface area, and external conditions where there is limited scope for significant design improvement. Therefore, the first step is critical for thermal-hydraulic design basis and better understanding of the internal passive heat transfer modes within the reactor systems can substantially improve design. Therefore, the confidence in the passive safety systems can be established by understanding and testing heat transfer processes from core in accident like situations for next generation reactors or improvised existing reactors. Most of the operating reactors across the world are water-cooled reactors and heat removal from the core is accompanied with sensible heat or latent heat transferred to water. Loss of Coolant Accident (LOCA) and associated severe accident scenarios in water-cooled reactors have been investigated for decades[45–49], resulting in models whos predictive accuracy is often contingent upon an understanding of complex two-phase flow phenomenon. Several next generation nuclear plants such as Small Modular Reactors, upcoming Generation III+ reactors, and existing nuclear power plants, have passive heat removal design capabilities for long-term decay heat removal with continuous natural circulation. In such designs, during the heat removal stage from core the coolant i.e. water is expected to change phase and get converted into steam. This steam or two-phase mixture with lower density will undergo natural upward draft and after being condensed on other equipment and structures in reactor system will flow downwards and complete the two-phase natural circulation path. The example designs of different passive safety systems such as isolation condensers (IC) and containment spray systems, shown here in Figures 5.1 and 5.2, are detailed in the IAEA report[2]. Isolation condensers are designed to provide cooling to BWR core, where the steam produced in the core is sent through the IC to condense and return to the core as a passive safety feature to continuously cool the core.

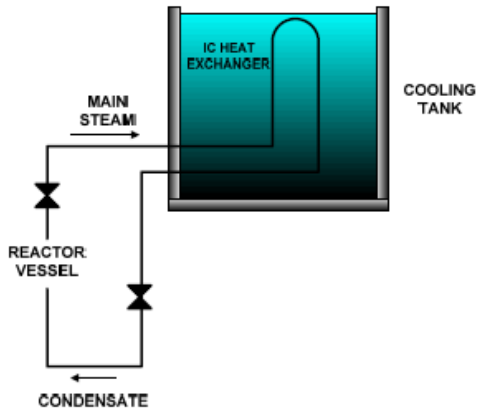

Figure 5.1: *Schematic of isolation condenser for a BWR*[2].

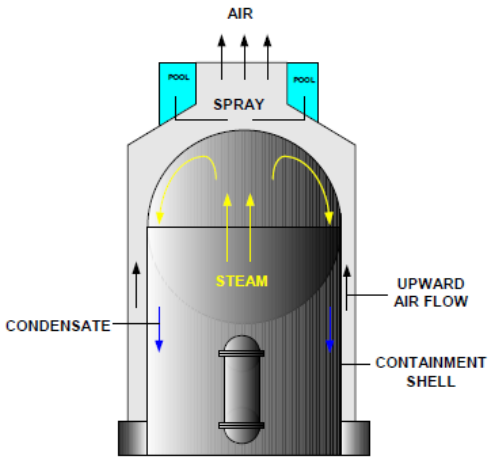

Figure 5.2: *Schematic of passive safety spray system and natural cooling draft air system for BWR*[2].

Similarly steam condensation on the containment walls of AP1000 reactor is important design feature to ensure the closed loop circulation after a break in coolant system. The condensed water can in turn be stored in reservoirs, which can be connected with IC heat exchanger loops or spray systems for continuous cooling of the core, primary coolant, and containment. Therefore, in all these examples the stable two phase natural circulation flow behavior is contingent upon steady, condensation-based heat rejection mechanism to a heat exchanger, containment walls, or any other geometrically complex system outside the reactor core. The already complex condensation process is accompanied with more complicated phenomenon such as transient thermal transport on containment walls, stratification of two phases, formation of discontinuous films etc.

5.2 Packed bed isolation condenser

A new packed bed isolation condenser design is proposed to reduce uncertainties in steam condensation process and improve passive heat removal capabilities of next generation LWRs. The packed bed isolation condenser comprises of small spherical alumina particles (1-3 mm diameter) which are chemically inert and have high energy density to act as long term heat sink. The schematic of packed bed isolation condenser with advanced BWR reactor is shown

in Figure 5.3, where the packed bed is isolated above and connected to the reactor vessel via closed valves. In the case of an emergency the top safety valve will open allowing the steam to flow through the pipe to enter the top of the packed bed and condense over the alumina particles into water. The condensate then exits the bottom of the packed bed and returns to the core by gravity completing the natural circulation loop. The heat rejected into the alumina particles will be slowly dissipated to the surroundings from naturally cooled walls of packed bed.

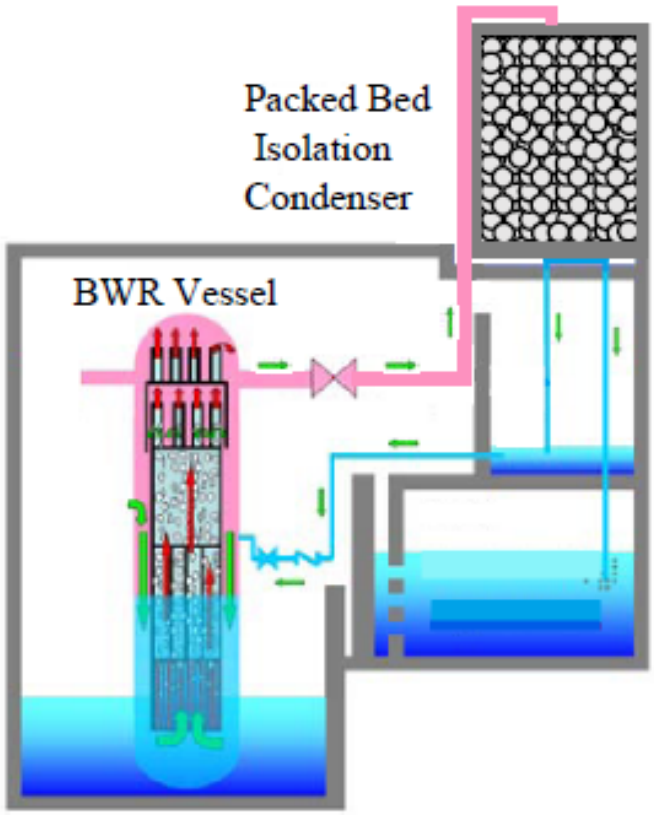

Figure 5.3: *Schematic of alumina packed bed isolation condenser for a BWR.*

The experimental studies on steam condensation in containment had spatial non-uniformities, which did not resolve the issues about reliability of design[50;51]. The prime need is to design a system where the vapor, steam, or two-phase mixture is expected to flow uniformly over the spatial domain and is expected to have higher degree of repeatability. As shown in previous chapter with different scale experiments and with high fidelity instrumentation, the steam

condensation on the packed beds is highly stable and continuous. The repeatability of the undertaken experiments and the quality of data obtained show that phase change or heat rejection process are uniform over the spatial domain as compared to condensation on the containment walls or water tanks.

Steam condenser designs rely upon indirect heat exchange with secondary fluid or external environment. Therefore their design parameters are obtained from steady state empirical correlations for steam condensation and two-phase flow. The conditions for steam or vapor condensation in the accident scenarios can be highly random, thus exact state of the fluid phase i.e. fraction of liquid entrained or stream pressures can vary. Therefore this packed bed system can be designed to handle more realistic scenarios where two phase mixture i.e. partially condensed steam can be the injection fluid stream. Heat transfer to the packed bed during the steam condensation in the vessel is expected to flow radially through the vessel walls to the environment, therefore internal heat resistance remains constant. This constant or stable internal heat resistance model during steam condensation in packed bed is expected to ensure steady condensate flow which can be collected and pumped back to the system under all circumstances.

5.3 Summary

A novel packed bed isolation condenser design is presented for passive heat removal in next generation LWRs to ensure steady condensation process and passive circulation. The data obtained from X-ray and IR camera images, and fiber optics based distributed temperature sensors of the experimental runs shown in previous chapter confirm that the steam condensation in the packed beds is highly stable, justifying the design basis. Steam condensation on walls and in tubes is often associated with spatial inhomogeneities which can lead to high degree of uncertainties. Uniform steam condensation on packed bed particles allow better spatial control over condensation process thereby increasing the reliability of passive safety system. However more quantitative analysis and scaling analysis is needed for the complete design proposition.

Chapter 6

Conclusions

Integration of TES systems can provide dispatch ability to NPPs and improve the economic scenario for nuclear power in future. The technical feasibility of this integration is conducted with the help of exergy and energy density analysis. The analysis for light water-cooled reactors shows that exergy recovery efficiency is around 90% and energy density values for the synthetic HTFs in this operating range are not expected to create practical challenges. The high temperature storage options, alumina packed beds and storage salt show exergy efficiency of 78% and 92%, respectively for advanced reactor concepts with high temperature non-light water coolants. Although both of these methods have thermodynamic potential, they can have practical compatibility limitations. For example, the compact layout of SMRs would not allow the integration of heat exchanger to be feasible. Therefore, direct recovery of thermal energy from steam into packed bed of rocks is proposed here. Analytical and experimental studies are conducted to understand thermal behavior of steam injection in packed beds.

The experimental results show that steam injection at different flow rates result in steep temperature gradients as compared to single phase heat transfer fluids such as air. Thermal gradients in the packed bed are governed by both conduction and advection effects. The conduction effects became apparent only in slow injection cases for thermocouples located away from the injection points as the steam front or the advection current take longer time to

reach those locations. Thus, the slope changes in the temperature dispersion curves become more apparent for slow injection cases. A semi-analytical physics based model was developed and compared with the experiments results. Validated model is then used to predict axial thermal dispersion in the beds. Axial dispersion is an important parameter used to design packed bed thermal energy storage systems, therefore its accurate measurement or prediction can dramatically improve the confidence level in the technology. Rayleigh-backscattering based distributed temperature sensing fiber optics system was deployed in the experimental scale and pilot scale geometries to obtain more precise measurement of axial dispersion than thermocouple arrangement. It can be concluded that during steam injection under all conditions or flow rates, the temperature front remains considerably steep, i.e. axial dispersion is minimal, as a function of time and position. With these studies it can be stated that packed bed thermal energy systems have a great potential of integration with systems where saturated steam is the only heat transfer fluid. With the stable condensation process observed in the packed beds, a novel passively safe isolation condenser design for advanced boiling water reactors is proposed. Future work on the deployment of these storage systems or evaluation of passive safe condensers require effect of higher pressure on the axial dispersion. For effective storage demonstration tests, a recovery cycle is also required at pilot scale which will be another critical task for future.

Bibliography

[1] *http://www.nuscalepower.com/.*

[2] IAEA. Passive Safety Systems and Natural Circulation in Water Cooled Nuclear Power Plants. 2009.

[3] *BNEF, 2014, https://www.iea.org/media/workshops/2014 /solarelectricity/bnef2lcoeofpv.pdf.*

[4] L. Borel and D. Favrat. *Thermodynamics and Energy systems analysis*, volume 1. 2010.

[5] P. Sabharwall, E.S. Kim, M. Mckellar, and M. Patterson. Small modular molten salt reactor (SM-MSR). *ASME 2011 Small Modular Reactors Symposium*, 2011.

[6] C. Forsberg and D. Curtis. Meeting the Needs of a Nuclear-Renewable Electrical Grid with a Fluoride-Salt-Cooled High-Temperature Reactor Coupled to a Nuclear Air-Brayton Combined Cycle Power System. *Nuclear Technology*, 2013.

[7] A. Bejan. Two thermodynamic optima in the design of sensible heat storage units for energy storage. *Journal of Heat Transfer*, 100:708–712, 1978.

[8] R.J. Krane. A second law analysis of the optimum design and operation of thermal energy storage systems. *International Journal of Heat and Mass Transfer*, 30:43–57, 1987.

[9] M. Wu, C. Li, C. Xu, Y. He, and W. Tao. The impact of concrete structure on the thermal performance of the dual-media thermocline thermal storage tank using concrete as the solid media. *Applied Energy*, 113:1363–1371, 2014.

[10] B. Xu, P. Li, and C. Chan. Application of phase change materials for thermal energy storage in concentrated solar thermal power plants: A review to recent developments. *Applied Energy*, 160:286–307, 2015.

[11] F.W. Schmidt and A.J. Willmott. Thermal Energy Storage and Regeneration. *Hemisphere Pub. Corp.*, 1981.

[12] M. Hanchen, S. Bruckner, and A. Steinfeld. High-temperature thermal storage using a packed bed of rocks-heat transfer analysis and experimental validation. *Applied Thermal Engineering*, 31, 2011.

[13] P. Klein, T. H. Roos, and T.J. Sheer. Parametric analysis of a high temperature packed bed thermal storage design for a solar gas turbine. *Solar Energy*, 118:59–73, 2015.

[14] A. Kere, V. Goetz, X. Py, R. Olives, and Sadiki N. Modeling and integration of a heat storage tank in a compressed air electricity stroage process. *Energy Conversion and Management*, 103:499–510, 2015.

[15] M. J. Doster, A. Rominger, and S. Bragg-Sitton. Reactor Subsystem Simulation for Nuclear Hybrid Energy Systems. *Idaho National Laboratory*, 2012.

[16] A. Bejan, G. Tsatsaronis, and M. Moran. Thermal design & optimization. 1996.

[17] B. Zalba, J.M. Marin, L.F. Cabeza, and H. Mehling. Review on thermal energy storage with phase change: materials, heat transfer analysis and applications. *Applied Thermal Engineering*, 23:251–283, 2003.

[18] S.M. Hasnain. Review on sustainable thermal energy storage technologies, part I: heat storage materials and techniques. *Energy Conversion and Management*, 39:1127–1138, 1998.

[19] S. Ball. Sensitivity Studies of Modular High-Temperature Gas-Cooled Reactor (MHTGR) Postulated Accidents. *Oak Ridge National Laboratory*, 2004.

[20] C. Andreades and P. Peterson. Technical Description of the "Mark 1" Pebble-Bed Fluoride-Salt-Cooled High-Temperature Reactor (PB-FHR) Power Plant. *Department of Nuclear Engineering, University of California, Berkeley*, 2014.

[21] U. Herrmann and D.W. Kearney. Survey of thermal energy storage for parabolic trough power plants. *Journal of Solar Energy Engineering*, 124:145–152, 2002.

[22] H. Bindra, P. Bueno, J. Morris, and R. Shinnar. Thermal analysis and exergy evaluation of packed bed thermal storage systems. *Applied Thermal Engineering*, 52:255–263, 2013.

[23] *Therminol-66 product specification- Company Catalog https://www.therminol.com/products/Therminol-66.*

[24] *Dowtherm-T product specification- Company Catalog http://www.dow.com/heattrans/products/synthetic/dowtherm.*

[25] M. Sohal, M. Ebner, P. Sabharwall, and P. Sharpe. Engineering Database of Liquid Salt Thermophysical and Thermochemical Properties. *Idaho National Laboratory*, 2010.

[26] R. Munro. Evaluated Material Properties for a Sintered alpha-Alumina. *Journal of American Ceramic Society*, 80:1919–1928, 1997.

[27] H. Bindra, P. Bueno, and J. Morris. Sliding flow method for exergetically efficient packed bed thermal storage. *Applied Thermal Engineering*, 54:201–208, 2014.

[28] D.E. Beasley and J.A. Clark. Transient response of a packed bed for thermal energy storage. *International Journal of Heat and Mass Transfer*, 27:1659–1669, 1984.

[29] D. Franken, J. Edwards, P. Sabharwall, and H. Bindra. Synthetic heat transfer fluids as thermal energy storage media for existing NPPs. *Transactions of American Nuclear Society*, Annual meeting 2016.

[30] J. Edwards, H. Bindra, and P. Sabharwall. Exergy Analysis of Thermal Energy Storage options with Nuclear Power Plants. *Annals of Nuclear Energy*, 96:104–111, 2016.

[31] Hitesh Bindra and Pablo Bueno. Optimum process design of packed bed type thermal storage systems and other applications, October 25 2016. US Patent 9,475,023.

[32] Reuel Shinnar and Hitesh Bindra. Thermal energy storage for combined cycle power plants, January 10 2017. US Patent 9,540,957.

[33] A. Testu, S. Didierjean, D. Maillet, C. Moyne, T. Metzger, and T. Niass. Thermal dispersion for water or air flow through a bed of glass beads. *International Journal of Heat and Mass Transfer*, 50:1469–1484, 2007.

[34] Y. James, J. Klausner, R. Mei, and J. Knight. Direct contact condensation in packed beds. *International Journal of Heat and Mass Transfer*, 49:4751–4761, March 2006.

[35] F. Alnaimat, J. Klausner, and R. Mei. Transient analysis of direct contact evaporation and condensation within packed beds. *International Journal of Heat and Mass Transfer*, 54:3381–3393, 2011.

[36] X. Li, S. Li, X. Cui, and H. Li. Experimental study of direct contact steam condensation in structured packing. *Asia-Pacific Journal of Chemical Engineering*, 8:657–664, 2013.

[37] A. Woods and S. Fitzgerald. The vaporization of a liquid front moving though a hot porous rock. Part 2. Slow injection. *Journal Fluid Mechanics*, 3443:303–316, 1997.

[38] C. Y. Wang and C. V. Beckermann. A two-phase mixture model of liquid-gas flow and heat transfer in capillary porous media-I. Formulation. *International Journal of Heat and Mass Transfer*, 36 (11):2747–2758, 1993.

[39] K. S. Udell. Heat transfer in porous media considering phase change and capillarity-the heat pipe effect. *International Journal of Heat and Mass Transfer*, 28 (2):485–495, 1985.

[40] Ryan Anderson, Samira Shiri, Hitesh Bindra, and Jeffrey F Morris. Experimental results and modeling of energy storage and recovery in a packed bed of alumina particles. *Applied Energy*, 119:521–529, 2014.

[41] J. F. Morris. Final Report-A Novel Storage Method for Concentrating Solar Power Plants Allowing Storage at High Temperature. *DOE Report*, OSTI 1158574, 2014.

[42] M. van Genutchen. Analytical solutions for chemical transport with simultaneous adsorption. Zero-order production and first-order decay. *Journal of Hydrology*, 49:213–233, 1981.

[43] A. Woods and S. Fitzgerald. The vaporization of a liquid front moving though a hot porous rock. *Journal Fluid Mechanics*, 251:563–579, 1993.

[44] I. Spiewak. Inherently Safe Reactors. *Annual Review of Energy and the Environment*, 10:431–462, 1985.

[45] F. Fichot, F. Duval, C. Trégourès, C. Béchaud, and M. Quintard. The impact of thermal non-equilibrium and large-scale 2D/3D effects on debris bed reflooding and coolability. *Nuclear Engineering and Design*, 236:2144–2163, 2006.

[46] F. Fichot, O. Marchand, P. Drai, P. Chatelard, M. Z. Ego, and J. Fleurot. Multi-Dimensional Approaches in Severe Accident Modelling and Analysis. *Nuclear Engineering and Technology*, 38(8):733–752, 2006.

[47] S. Leininger, R. Kulenovic, S. Rahman, G. Repetto, and E. Laurien. Experimental investigation on reflooding of debris beds. *Annals of Nuclear Energy*, 74:42–49, 2014.

[48] L. Li, W. Ma, and S. Thakre. An experimental study on pressure drop and dryout heat flux of thwo-phase flow in packed beds of multi-sized and irregular particles. *Nuclear Engineering and Design*, 242:369–378, 2012.

[49] W. Ma, R. Hansson, L. Li, and P. Kudinov. In-vessel Coolability and Steam Explosion in Nordic BWRs. 2010.

[50] M. H. Anderson, L. E. Herranz, and M. L. Corradini. Experimental analysis of heat transfer within the AP600 containment under postulated accident conditions. *Nuclear Engineering and Design*, 185:153–172, 1998.

[51] L. E. Herranz, M. H. Anderson, and M. L. Corradini. A diffusion layer model for steam condensation within the AP600 containment. *Nuclear Engineering and Design*, 183: 133–150, 1998.